Biomedicine & Pharmacotherapy 152 (2022) 113270

Contents lists available at ScienceDirect

Biomedicine & Pharmacotherapy

journal homepage: www.elsevier.com/locate/biopha

Targeting cholesteryl ester accumulation in the heart improves cardiac insulin response

Virginia Actis Dato [a,b,1], Aleyda Benitez-Amaro [c,d,1], Eduardo Garcia [c,d,1], Lene Claudi [c,d], Maria Teresa LaChica Lhoëst [c,d], Antoni Iborra [e], Joan Carles Escola-Gil [f], Jose Maria Guerra [g,h], Valerie Samouillan [i], Carlos Enrich [j,k], Gustavo Chiabrando [a,b,*,2], Vicenta Llorente-Cortés [c,d,h,**,3]

[a] Departamento de Bioquímica Clínica, Facultad de Ciencias Químicas, Universidad Nacional de Córdoba, Argentina
[b] Consejo Nacional de Investigaciones Científicas y Técnicas (CONICET), Centro de Investigaciones en Bioquímica Clínica e Inmunología (CIBICI), Córdoba, Argentina
[c] Institute of Biomedical Research of Barcelona (IIBB)-Spanish National Research Council (CSIC), Barcelona, Spain
[d] Biomedical Research Institute Sant Pau (IIB Sant Pau), Barcelona, Spain
[e] SCAC, Universitat Autònoma de Barcelona (UAB), Bellaterra, Spain
[f] Metabolic Basis of Cardiovascular Risk, Biomedical Research Institute Sant Pau (IIB Sant Pau), Hospital de la Santa Creu i Sant Pau. CIBER de Diabetes y enfermedades Metabólicas Asociadas (CIBERDEM), Barcelona. Spain
[g] Department of Cardiology, Hospital de la Santa Creu i Sant Pau, Biomedical Research Institute Sant Pau (IIB Sant Pau), Universitat Autonoma de Barcelona, Barcelona, Spain
[h] CIBERCV, Institute of Health Carlos III, 28029 Madrid, Spain
[i] CIRIMAT, Université de Toulouse, Université Paul Sabatier, Equipe PHYPOL, 31062 Toulouse, France
[j] Unitat de Biologia Cel·lular, Departament de Biomedicina, Facultat de Medicina i Ciències de la Salut, Universitat de Barcelona, Barcelona, Spain
[k] Centre de Recerca Biomèdica CELLEX, Institut d'Investigacions Biomèdiques August Pi i Sunyer (IDIBAPS), Barcelona, Spain

ARTICLE INFO

Keywords:
High-fat diet
Lipid droplets
Cholesteryl esters
Heart
Lipoprotein
Insulin
LRP1

ABSTRACT

Background: Antibodies against the P3 sequence (Gly1127-Cys1140) of LRP1 (anti-P3 Abs) specifically block cholesteryl ester (CE) accumulation in vascular cells. LRP1 is a key regulator of insulin receptor (InsR) trafficking in different cell types. The link between CE accumulation and the insulin response are largely unknown. Here, the effects of P3 peptide immunization on the alterations induced by a high-fat diet (HFD) in cardiac insulin response were evaluated.

Methods: Irrelevant (IrP)- or P3 peptide-immunized rabbits were randomized into groups fed either HFD or normal chow. Cardiac lipid content was characterized by thin-layer chromatography, confocal microscopy, and electron microscopy. LRP1, InsR and glucose transporter type 4 (GLUT4) levels were determined in membranes and total lysates from rabbit heart. The interaction between InsR and LRP1 was analyzed by immunoprecipitation and confocal microscopy. Insulin signaling activity and glucose uptake were evaluated in HL-1 cells exposed to rabbit serum from the different groups.

Findings: HFD reduces cardiac InsR and GLUT4 membrane levels and the interactions between LRP1/InsR. Targeting the P3 sequence on LRP1 through anti-P3 Abs specifically reduces CE accumulation in the heart independently of changes in the circulating lipid profile. This restores InsR and GLUT4 levels in cardiac membranes as well as the LRP1/InsR interactions of HFD-fed rabbits. In addition, anti-P3 Abs restores the insulin signaling cascade and glucose uptake in HL-1 cells exposed to hypercholesterolemic rabbit serum.

* Correspondence to: Departamento de Bioquímica Clínica, Facultad de Ciencias Químicas, Universidad Nacional de Córdoba, Haya de la Torre s/n, Ciudad Universitaria, 5000 Córdoba, Argentina.
** Correspondence to: Institute of Biomedical Research of Barcelona (IIBB)-Spanish National Research Council (CSIC), Biomedical Research Institute Sant Pau (IIB Sant Pau), Sant Quintí 77-79, 08041 Barcelona, Spain.
E-mail addresses: gustavo.chiabrando@unc.edu.ar (G. Chiabrando), vicenta.llorente@iibb.csic.es, cllorente@santpau.cat (V. Llorente-Cortés).
[1] These authors equally contributed to this work
[2] ORCID: 0000-0001-8902-6693
[3] ORCID: 0000-0001-8591-7632

https://doi.org/10.1016/j.biopha.2022.113270
Received 4 May 2022; Received in revised form 2 June 2022; Accepted 6 June 2022
Available online 13 June 2022

Interpretation: LRP1-immunotargeting can block CE accumulation within the heart with specificity, selectivity, and efficacy, thereby improving the cardiac insulin response; this has important therapeutic implications for a wide range of cardiac diseases.
Funding: Fundació MARATÓ TV3: grant 101521-10, Instiuto de Salud Carlos III (ISCIII) and ERDF PI18/01584, Fundación BBVA Ayudas a Equipos de Investigación 2019. SECyT-UNC grants PROYECTOS CONSOLIDAR 2018-2021; FONCyT, Préstamo BID PICT grant 2015-0807 and grant 2017-4497.

1. Introduction

Cardiovascular disease (CVD) is the leading cause of death worldwide and is frequently associated with metabolic syndrome (MS) and type 2 diabetes mellitus (T2DM)[1–4]. Individuals with MS or T2DM have a 2.5-times higher risk of developing heart failure than healthy individuals [5], and frequently present myocardium steatosis, which is associated with alterations in insulin signaling [6–8] and precedes diastolic dysfunction and loss of metabolic flexibility [9–11]. Further, insulin resistance is associated with pathological remodeling of the heart, which is characterized by concentric hypertrophy of the left ventricle, interstitial fibrosis, and extracellular matrix (ECM) remodeling that leads to diastolic dysfunction [12–14]. Recently, left ventricle myocardial remodeling has been linked to high levels of cholesteryl ester (CE)-enriched lipoproteins, such as low-density lipoprotein (LDL), using paired lipid and cardiovascular magnetic resonance data, in a one-sample Mendelian randomization study that included 17 311 individuals [15]. However, the molecular mechanisms underlying the link between lipoprotein-derived cardiac lipid accumulation, insulin action, and cardiac dysfunction are largely unknown.

The susceptibility of LDL particles to aggregate is associated with increased cardiovascular mortality [16]. The small, dense LDL particles (prevalent in MS and T2DM patients) have a higher tendency to be retained and aggregated (agLDL) in the extracellular spaces of several tissues, including the arterial intima [17–19]. AgLDL, in contrast to native LDL, is taken up by the LDL receptor-related protein 1 (LRP1), a receptor that is upregulated by hypercholesterolemic conditions in cells of the cardiovascular system (including smooth muscle cells, macrophages, and cardiomyocytes) [20–22]. The interaction of LRP1 with agLDL facilitates the selective uptake and transfer of CEs from agLDL to intracellular lipid droplets of vascular and cardiac cells [21,22]. Of note, LRP1-mediated agLDL uptake decreases insulin-induced intracellular signaling, glucose transporter type 4 (GLUT4) translocation to the plasma membrane, and glucose uptake by HL-1 cells [6]. In fat and muscle cells, LRP1 regulates the intracellular trafficking of insulin-responsive GLUT4 storage vesicles (GSV) [23]. Under insulin stimulation, GSVs are trafficked and fused with the plasma membrane by a mechanism that is dependent on the activation of the phosphatidylinositol-3-kinase (PI3K)/protein kinase B (Akt)/AS160 (Akt substrate of 160 kDa) pathway [24]. LRP1 interacts with insulin receptor (InsR) to regulate InsR-associated intracellular signaling in neurons, hepatocytes, and cardiomyocytes [6,25,26]. In addition, in retinal Müller glial cells, blocking LRP1 exocytosis towards the plasma membrane disturbs intracellular signaling induced by insulin[27]. These data suggest that LRP1 is critical for the link between lipid accumulation and insulin signaling in different cell types.

The LRP1 P3 peptide sequence of H-GDNDSEDNSDEENC-NH2 (Gly1127–Cys1140) is located on the CR9 domain of the extracellular alpha chain, cluster II and is crucial for the interaction of this receptor with CE-enriched lipoproteins [28]. We previously showed that polyclonal antibodies against the P3 sequence (anti-P3 Abs) efficiently reduced foam cell formation and atherosclerosis in *in vitro*, *ex vivo,* and *in vivo* models [28,29]. In particular, purified anti-P3 Abs have a higher affinity for the P3 epitope than agLDL, blocking the binding of this atherogenic LDL to LRP1 and its subsequent uptake by vascular cells [28]. In *in vivo* studies, immunization against LRP1 prevents intracellular CE accumulation in the vasculature and harmful coupling of pro-inflammatory signaling in rabbits, as well as in *ex vivo* human macrophages or human coronary vascular smooth muscle cells exposed to rabbit hypercholesterolemic sera [29]. The CR9 domain (which binds anti-P3 Abs) show scarce affinity for serpins, such as plasminogen activator inhibitor-1 and protease nexin 1, which induce a protective signal in the heart [30]. This makes CR9 an ideal target for blocking LRP1 interactions with pathological ligands (atherogenic lipoproteins) but without altering interactions with protective ligands (protease-inhibitor complexes) [31]. On the basis of these previous results, the main objectives of the present study were i) to evaluate the impact of CE-enriched lipoproteins on cardiac lipid accumulation, and ii) to study the consequences of CE accumulation on cardiac insulin response. For this, we specifically blocked the interaction of CE-enriched lipoproteins with LRP1 receptor *via* immunization with the peptide P3.

2. Methods

2.1. Animal model

Experimental procedures were approved by the Ethics Committee of Animal Experimentation of the Vall d'Hebron Institute of Research with registration number 46/17, and performed in accordance with Spanish legislation and also with the European Union directives (2010/63/ EU). Female rabbits (thirty New Zealand White [NZW]) were fed i) a chow R-01 diet from Granja San Bernardo with the following formulation: 17.3 % protein, 16.7 % fiber, and 3 % fat, or ii) a high-fat diet (HFD) TD.88 137 (42 % fat, 0.2 % cholesterol) from ENVIGO, for 1 month (Fig. S1a). Animals were acclimated for one week before the first immunization and immunized with a primary injection and four reminder doses (R1-R4) every 21 days of irrelevant peptide (IrP group; $n = 10$) or P3 peptide (P3 group; $n = 10$) conjugated to the carrier. The four doses of IrP or P3 antigen conjugated with keyhole limpet hemocyanin (KLH) were administered subcutaneously (138 μg/kg, maximum volume 150 μl). For the first immunization, IrP or P3-KLH peptides were emulsified in complete Freund's adjuvant; the rest of the immunizations were done using IrP or P3-KLH conjugated in incomplete Freund's adjuvant (both from Sigma Aldrich). During the immunization period, the animals were fed a normal chow diet. Starting at the R4 time point, IrP- and P3-immunized rabbits were randomly divided into a chow-fed or a HFD-fed group. Ten rabbits ($n = 5$ IrP-injected, $n = 5$ P3-injected) continued the chow diet, whereas ten rabbits ($n = 5$ IrP-injected, $n = 5$ P3-injected) received HFD for 30 days. Four groups of rabbits were included in this study: i) chow IrP-immunized, ii) chow P3-immunized, iii) HFD IrP-immunized, and iv) HFD P3-immunized (Fig. S1a). Animals were weighed at pre- and post-diet time points, and serum levels of specific anti-P3 antibodies were determined by ELISA. At the end of the study, animals were euthanized, and the hearts and livers were removed aseptically and processed for molecular, confocal, electron microscopy, biophysical, and immunohistochemical studies.

2.2. Peptide synthesis and conjugation

The P3 peptide used to immunize rabbits contained the sequence GDNDSEDNSDEENC, which corresponds to the amino acids 1127–1140 located in LRP1 cluster II (domain CR9) [28,29]. The P3 sequence corresponds to an area of high homology between human and rabbit LRP1, with the difference that the asparagine (N) in humans was replaced by a

serine (S) in the rabbit protein. In addition, the amino acid C1140 in the rabbit sequence (GDNDCEDNSDEENC) was replaced by S to achieve greater peptide immunogenic effectiveness. The irrelevant peptide (IrP) has the same sequence than P3 but with amino acids in D-enantiomer configuration. Both peptides were synthesized by the Laboratory of Proteomics & Protein Chemistry, Department of Experimental & Health Sciences, Pompeu Fabra University, by the solid-phase method using a Prelude peptide synthesizer (Protein Technologies, Inc.). Peptides were purified by high-performance liquid chromatography (HPLC, Waters 600) using UV detection at 254 nanometers (Waters 2487) and characterized by mass spectrometry (Applied Biosystems 4700 Proteomics Analyser). Peptide conjugation to KLH or BSA (Sigma, St. Louis, MO) was performed as previously described [32]. Peptide–KLH conjugates were used for rabbit immunization, and peptide-BSA conjugates were used as a substrate in the immunoassay ELISA to detect specific anti-P3 Abs in the rabbit serum.

2.3. Detection of specific antibodies

ELISAs were standardized to detect specific antibodies against P3 peptides. Briefly, all sera were analyzed using 96-well polystyrene plates (442 404 Maxisorp, NUNC, Labclinics, Spain) coated with peptide-BSA or BSA as a control to detect unspecific antibodies. ELISA plates were incubated with several serum dilutions for 90 min; after washes, anti-rabbit IgGs conjugated to peroxidase (170–6515, BioRad, Spain) were added to detect the antigen–antibody complexes. ELISA was revealed using OPD substrate (P9187, Sigma Aldrich, Spain), and the absorbance was read in a Multilabel reader Victor3 (Perkin Elmer, Turku, Finland) at 450 nm. The measured absorbances were adjusted to a 4PL curve to calculate the IC50. The parameter 1/IC50 was used as the antibody titer.

2.4. Biochemical analysis of serum and isolated lipoproteins

Serum lipids and lipoproteins, including cholesterol and triglyceride (TG) (corrected from free glycerol), were enzymatically determined using commercial kits adapted to a COBAS 6000 autoanalyzer (Roche Diagnostics) [33]. VLDL, LDL, and HDL lipoproteins were isolated by sequential ultracentrifugation at 100,000*g* for 24 h at a density of 1.006, 1.019–1.063 and 1.063–1.21 g/ml, respectively, using an analytical fixed angle rotor (50.3, Beckman Coulter). The composition of each lipoprotein, including total and free cholesterol, triglycerides and phospholipids, was determined by commercial methods adapted to the COBAS 501 autoanalyzer. Lipoprotein protein concentrations were determined by the bicinchoninic acid method (Termo Scientific, Rockford, IL). Lipid and protein concentrations were used to calculate the total mass of each lipoprotein.

2.5. Glucose tolerance test (GTT)

The glucose tolerance test (GTT) was performed at week four of the dietetic intervention under fasting conditions. Basal blood glucose levels were measured from an ear nick through ACCU-CHEK® Aviva glucometer (Roche Molecular Systems). Rabbits were then intraperitoneally injected with glucose (1.3 mg/g BW). Blood glucose was measured at 15 min, 30 min, 60 min, 120 min and 180 min after glucose injection. The area under the curve (AUC) of the response curve was then calculated using the software Prism 4.0 [34].

2.6. Cell culture

The murine HL-1 cardiomyocyte-derived cell line was generated by Dr. W.C. Claycomb (Louisiana State University Medical Centre, New Orleans, Louisiana, USA). HL-1 cells were maintained in Claycomb medium (Sigma-Aldrich) in plastic dishes [6], coated with 12.5 g/ml fibronectin (Sigma-Aldrich) and 0.02 % gelatin, in a 5% CO2 atmosphere at 37 °C. HL-1 cells were fasted with 0.2 % FBS for 24 h and then were incubated with serum (0.25 %, 1.5 h) from the different rabbit groups i) chow IrP-immunized, ii) chow P3-immunized, iii) HFD IrP-immunized, and iv) HFD P3-immunized-rabbits.

2.7. Determination of neutral lipid content in heart and liver

Myocardial, hepatic, and cellular lipids were extracted and partitioned by thin-layer chromatography. Lipids were extracted with dichloromethane/methanol [1:2] and cholesteryl esters (CE), free cholesterol (FC), and triglycerides (TG) were analyzed by thin-layer chromatography (TLC) on silica G-24 plates as previously described [35,36]. Different concentrations of standards (a mixture of cholesterol, cholesterol palmitate and triglycerides) were applied to each plate. The spots corresponding to CE, TG, and FC were quantified by densitometry against the standard curve of cholesterol palmitate, triglycerides and cholesterol, respectively, using a computing densitometer.

2.8. Assessment of lipid droplet morphology and size

2.8.1. Electron microscopy

Cells growing in 60 mm plates were washed in PBS 1X and then fixed with 2.5 % glutaraldehyde in 0.1 M phosphate buffer at room temperature for 1 h. Next, cells were gently scraped and then pelleted in 1.5 ml tubes. Cardiac tissue was cut into small pieces, extensively washed in PBS 1X and fixed with 2.5 % glutaraldehyde, 2 % PFA in 0.1 M phosphate buffer overnight. Samples were dehydrated, embedded in Spurr and sectioned using Leica ultramicrotome (Leica Microsystems). Ultrathin sections (50–70 nm) were stained with 2 % uranyl acetate for 10 min, a lead-staining solution for 5 min and then analyzed with a transmission electron microscope, JEOL JEM-1010 fitted with a Gatan Orius SC1000 (model 832) digital camera at the Unit of Electron Microscopy, Scientific and Technological Centers of the University of Barcelona, School of Medicine and Health Sciences (Barcelona, Spain).

2.8.2. Confocal microscopy

A stock solution of the fluorescent dye boron-dipyrromethene (BODIPY) was diluted to a final concentration of 1 mg/ml in DMSO. To study lipid droplets, heart slides were incubated for 30 min with 100 μl of BODIPY (1 mg/ml in DMSO). Images of immunostained cells were analyzed on a Leica inverted fluorescence confocal microscope (Leica TCS SP2-AOBS; excitation wavelength 480 nm, emission maximum 515 nm).

2.9. FTIR, freeze-dried state

Fourier transform infrared spectroscopy/attenuated total reflectance (FTIR/ATR) spectra of the freeze-dried lipoproteins and tissues were acquired using a Nicolet 5700 FTIR instrument (Thermo Fisher Scientific, Waltham, MA) equipped with an ATR device with a KBr beam splitter and a MCT/B detector as previously described [37,38]. The ATR accessory used was a Smart Orbit with a type IIA diamond crystal (refractive index 2.4). Freeze-dried samples (1 mg) were directly deposited on the entire active surface of the crystal and gently pressed with a Teflon tip to assure good contact. For each sample, 80 interferograms were recorded in the 4000–450/cm-1 region, co-added and Fourier transformed to generate an average spectrum of the segmented heart part with a nominal resolution of 1 cm-1 using Omnic 8.0 (Thermo Fisher Scientific, Waltham, MA). A single-beam background spectrum was collected from the clean diamond crystal before each experiment, and this background was subtracted from the spectra. Spectra were then subjected to ATR and baseline corrections and normalized using the maximum of the Amide II peak. Second derivatives were used to enhance the chemical information present in overlapping infrared absorption bands of spectra.

2.10. Determination of InsR and LRP1 levels in membranes and total cardiac lysates

2.10.1. Tissue subfractionation

Tissue was washed with PBS 1X and homogenized using a POLYTRON® Immersion Dispersers PT 2500 as previously described [35,38]. In brief, to obtain membrane protein fraction, the homogenized tissue was filtered using QIAshredder spin columns (79 656, QIAGEN), incubated with lysis buffer A (NaCl 150 mM, HEPES 50 mM, digitonin 25 μg/ml, 1 M hexylene glycol, protease inhibitor cocktail 1 % v-v) using an end-over-end rotator. After centrifugation, the supernatant containing mainly cytosolic proteins was removed and the the pellet was incubated with lysis buffer B (NaCl 150 mM, HEPES 50 mM, igepal 1 % v-v, 1 M hexylene glycol, protease inhibitor cocktail 1 % v-v). After centrifugation, the supernatant containing mainly plasma membrane proteins was collected. Proteins were analyzed by Western blot with antibodies against rabbit LRP1 (ab92544 Abcam) or InsR (LS-C63091, LSBio) or GLUT4 (LS-C123618, LSBio). Total cardiac lysates were obtained using RIPA buffer (50 mM Tris-HCl pH 8.0, 150 mM NaCl, 1 % Triton X-100, 0.5 % sodium deoxycholate, 0.1 % SDS, 1 mM PMSF, 10 mM sodium ortho-vanadate, and protease inhibitor cocktails (Sigma-Aldrich, St. Louis, MO, USA), and proteins were analyzed by Western blot. Anti-ATP1A1 (MA3–928, Invitrogen) and anti-GAPDH (sc-81 545, Santa Cruz Biotechnology) were used as total and plasma membrane loading controls, respectively.

2.10.2. Biotin-labeling of cell surface proteins

HL-1 cells were exposed to rabbit's serum (0.25 %) for 1.5 h and then treated with insulin (100 nM) for 30 min. Biotin-labeling protein assay (EZ-Link Sulfo-NHS-SS-Biotin (21 331,Thermo Scientific) was used to determine the protein levels of GLUT4 at the cell surface. Briefly, cells were incubated first with a biotin solution 0.12 mg/ml for 2 h at 4 °C and, then with 0.1 mM glycine solution for 30 min at 4 °C and then washed three times with PBS 1X. Biotinylated proteins were pulled down by streptavidin-conjugated agarose beads (Pierce Streptavidin Agarose (20 353, Thermo Scientific) for 2 h at room temperature. Biotinylated and total proteins (10 % of proteins incubated with agarose beads) were analyzed by Western blot after incubated with rabbit anti-GLUT4 (sc-7938; Santa Cruz Biotechnology), mouse monoclonal anti-ATP1A1 (MA3–928, Invitrogen), or mouse monoclonal anti-β-actin (A2228; Sigma-Aldrich) antibodies overnight at 4 °C, following by incubation with secondary antibodies (goat anti-mouse and goat anti-rabbit; Dako) diluted 1/10 000 for 1 h at room temperature. Signals were detected with the ECL immunoblotting detection system (GE Healthcare) and results were quantitatively analyzed using Chemidoc (BioRad). Biotinylated-ATP1A1 and β-actin were used as loading control of plasma membrane protein and total protein extracts, respectively.

2.11. Western blot analysis

Protein extracts were obtained using RIPA buffer (50 mM Tris-HCl pH 8.0, 150 mM NaCl, 1 % Triton X-100, 0.5 % sodium deoxycholate, 0.1 % SDS, 1 mM PMSF, 10 mM sodium ortho-vanadate, and protease inhibitor cocktails) (Sigma-Aldrich, St. Louis, MO, USA). Cell protein extracts (40 μg) were diluted in 5 × sample buffer with dithiothreitol (DTT) and heated for 5 min at 95 °C. Electrophoresis on 10 % SDS-polyacrylamide gels was performed, and proteins were transferred to nitrocellulose membrane (GE Healthcare Life Science, Amsterdam, The Netherlands). Nonspecific binding was blocked with 5 % non-fat dry milk in a Tris-HCl buffer containing 0.01 % Tween 20 (TBS-T) for 60 min at room temperature. Membranes were incubated overnight at 4 °C with primary antibodies and then with secondary antibodies (goat anti-mouse and goat anti-rabbit; Dako) diluted 1/10 000 for 1 h at room temperature. For signaling activation analysis, the following primary antibodies were used: rabbit anti-Akt (9272, Cell Signaling Technology), rabbit anti-pAkt (Ser473, 07–789, Merck), rabbit anti-AS160 (ab24469, Abcam), rabbit anti-pAS160 (Thr642, ab65753, Abcam), and mouse monoclonal anti-β-actin (A2228; Sigma-Aldrich). Signals were detected with the ECL immunoblotting detection system (GE Healthcare), and the results were quantitatively analyzed using Chemidoc (BioRad).

2.12. Confocal microscopy

The procedures were followed as previously described [6]. HL-1 cardiomyocyte were washed with PBS 1 × , fixed with 4 % paraformaldehyde (PFA), permeabilized for 30 min with 0.5 % (v/v) saponin and blocked with 2 % bovine serum albumin (BSA). Primary antibodies were used for 1 h, using rabbit anti-LRP1 monoclonal antibody (ab92544, Abcam) or mouse anti-InsR antibody (ab69508; Abcam), and secondary antibodies conjugated with Alexa Fluor (1/800) and Hoechst 33 258 (1/2000) were used for 1 h. Finally, cells were mounted with Mowiol 4–88 (Calbiochem (Merck, Darmstadt). Images were obtained with an Olympus FluoView FV1200 confocal microscope (Olympus), processed using the FV10-ASW Viewer 3.1 (Olympus) and quantified by ImageJ software. Quantification of the colocalization level was analyzed by JACoP plug-in from ImageJ software [6].

Heart slides were washed with PBS 1 × , permeabilized for 5 min with PBS 1 × with 1 % Tween and blocked with PBS 1 × with 1 % BSA. Primary antibodies were used for 1 h (mouse anti-GLUT4 monoclonal antibody LS-C123618. LS-Bio) (1/50) and secondary antibody conjugated with alexa fluor (1/100) and Hoechst 33 258 (1/1000) were used for 1 h. Slides were then mounted with ProLong™ Gold Antifade Mountant (P10144, Thermoscientific). Images were obtained with an Olympus FluoView FV1200 confocal microscope (Olympus), processed using the FV10-ASW Viewer 3.1 (Olympus) and quantified by ImageJ software.

2.13. Immunoprecipitation (IP) assay

Cardiac tissue from the rabbit groups and HL-1 cells exposed to rabbit's serum from each of the four groups were subjected to immunoprecipitation (IP) assays as previously described [6]. Briefly, protein extracts were incubated with rabbit anti-LRP1 monoclonal antibody (ab92544, Abcam) or rabbit non-immune IgG as control (2 μg/200 μg of total proteins) for 2 h at 4 °C. Samples were then incubated with protein A–conjugated agarose agarose beads following the manufacturer's procedure (sc-2001; Santa Cruz Biotechnology) overnight at 4 °C. Immunoprecipitated proteins were characterized by Western blot using anti-InsR (ab69508; Abcam) and anti-LRP1 (ab92544; Abcam) monoclonal antibodies, and secondary antibodies (goat anti-mouse or goat anti-rabbit; Dako). Signals were detected using ECL immunoblotting detection system (GE Healthcare) and the results were quantitatively analyzed using Chemidoc (BioRad).

2.14. 2-NBDG uptake assay

HL-1 cells were exposed to rabbit's serum (0.25 %) for 1.5 h and then treated with insulin (100 nM) in the presence of 2-deoxy-2-[(7-nitro-2,1,3-benzoxadiazol-4-yl) amino]-D-glucose (2-NBDG solution; Sigma-Aldrich) (80 μM) for 30 min. Cells were then washed with 1X PBS, fixed with 4 % paraformaldehyde, blocked with 2 % BSA, and incubated with Hoechst 33 258 colorant (1/2000) for 1 h [6]. Fluorescence was detected with a Leica DMI8 biological microscope (Leica, Germany). Total fluorescence in the whole cell area was quantified by ImageJ software.

2.15. Statistical analysis

Differences between study groups were analyzed using two-way analysis of variance (ANOVA) followed by a Tukey *post-hoc* test. The statistical software R (www.r-project.org) was used for all statistical analyses. Differences were considered statistically significant when $p <$

0.05.

3. Results

3.1. Immunization with the P3 peptide produces anti-P3 Abs in rabbits

The experimental rabbit immunization procedure included the primary injection and four booster injections of either the P3 peptide or an irrelevant peptide (IrP), and two blood extractions at the checking points. Rabbits were either fed a high-fat diet (HFD) or a control diet (*i.e.*, normal chow) for 30 days (Fig. S1a). ELISA analysis showed a significant anti-P3 Abs production that was maintained throughout the entire dietetic intervention period in the serum of P3-immunized rabbits, based on the levels of antibodies at the two checkpoints, Chk1 and Chk2 (Fig. S1b, middle and left panel). Rabbits immunized with the IrP peptide did not show any response against P3 in ELISA (Fig. S1c).

3.2. Lipid profile and peripheral insulin resistance induced by HFD are not modified by anti-P3 Abs

Cholesterol levels (Fig. 1a) and triglyceride (TG) levels (Fig. 1b) were higher in the serum of HFD-fed rabbits than in serum of control diet rabbits, with no differences between P3- or IrP-immunized rabbits. Liver lipid extraction followed by TLC showed a significant upregulatory effect of HFD on levels of hepatic CE, TG, and free cholesterol (FC), also with no differences between P3- or IrP-immunized rabbits (Fig. 1c-f).

Rabbits in all four groups (*e.g.*, HFD P3, HFD IrP, chow P3, and chow IrP) exhibited a similar increase in body weight over the study period (30 days) (Fig. S2a). However, the glucose tolerance test (GTT) showed that HFD induced glucose intolerance in both IrP and P3 immunized groups (Fig. S2b, c), indicating that the impairment of peripheral insulin response induced by HFD was not affected by P3 immunization.

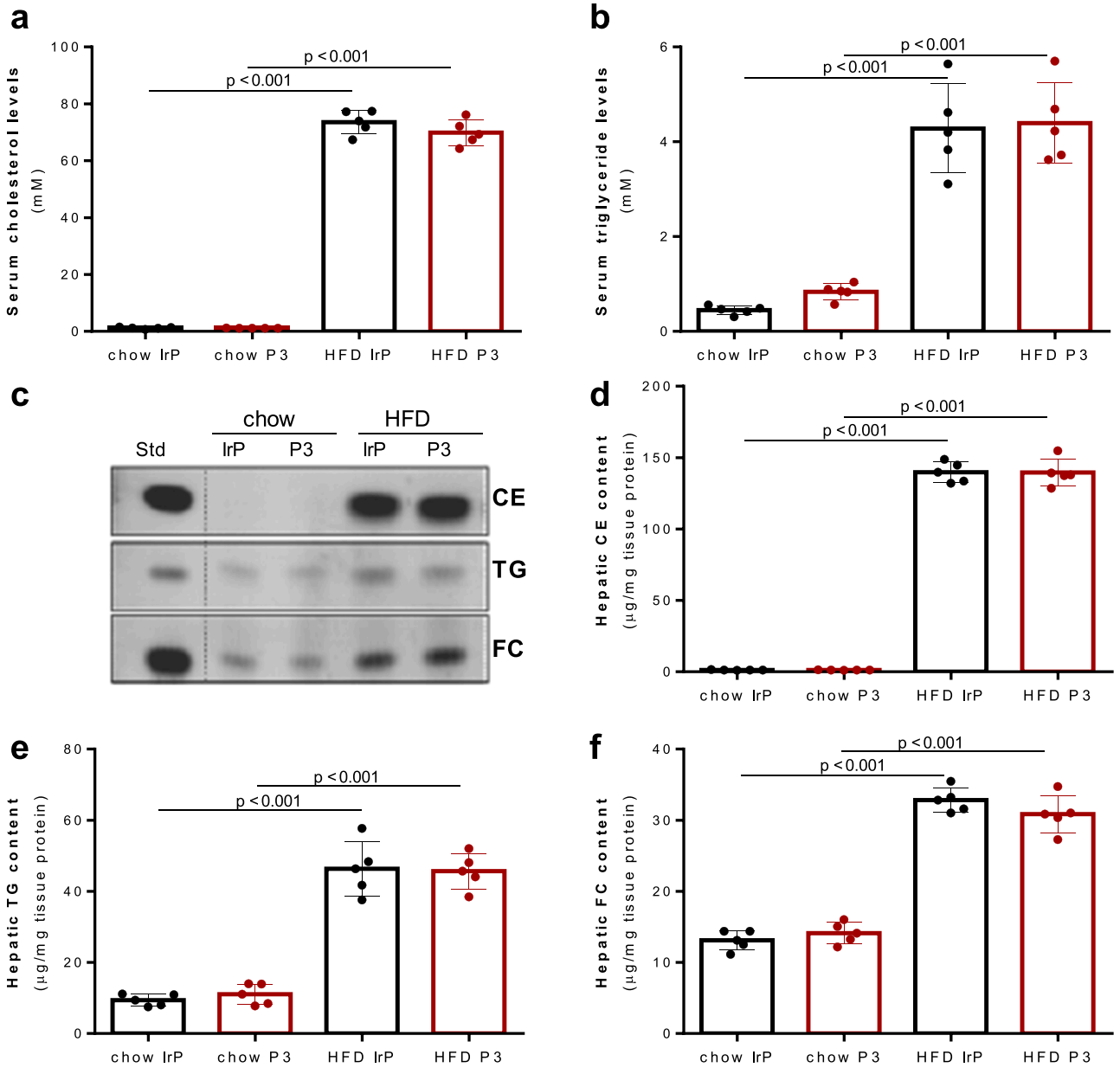

Fig. 1. Immunization with P3 peptides does not alter serum or liver lipid profiles in rabbits. (a, b) Bar graphs showing serum cholesterol and triglyceride (TG) levels. (c) Representative thin-layer chromatography (TLC) of cholesterol ester (CE), TG, and free cholesterol (FC) in the liver. The CE/TG/FC bands from the standards (Std) are shown. (d, e, f) Bar graphs showing results as mean ± SD of CE, TG, or FC, quantified as µg/mg tissue protein. Statistical significance was determined by 2-way ANOVA with Tukey's post-hoc test. $n = 5$/group.

3.3. Cholesteryl esters in HFD-fed rabbits are mainly carried by VLDL and LDL lipoproteins

The HFD-fed groups had much higher total mass of circulating LDL (IrP: 32.10 ± 3.53 *vs* 1.23 ± 0.68 g/L, $p < 0.001$) and, to a lesser extent, of VLDL (IrP: 5.90 ± 0.85 *vs* 0.35 ± 0.13 g/L, $p < 0.001$), than either of the chow-fed groups (Fig. S3), with most of HFD-increased plasma cholesterol carried by LDL and VLDL. Both VLDL and LDL had much higher CE content in HFD rabbits (Fig. S3c,d) than in control rabbits (Fig. S3a,b), with no differences in the lipid/protein profile of VLDL and LDL lipoproteins between IrP- and P3-injected rabbits, irrespective of diet. Despite the low total mass of circulating VLDL and LDL in serum from control groups, these lipoproteins had higher proportion of TG (Fig. S3a,b) than the HFD groups (Fig. S3c,d), irrespective of IrP- or P3-immunization. HDL was the minor lipoprotein class, with a similar composition in the four groups. Overall, the lipoprotein fraction content of VLDL, LDL, and HDL lipoprotein masses, as well as of TG, phospholipid (Ph), FC, CE, and protein levels, were similar between IrP- and P3-injected groups irrespective of diet. These results clearly indicate that P3 immunization did not significantly alter the lipid/protein profile of VLDL, LDL, or HDL in rabbits.

3.4. The spectral FTIR lipid signature of CE-enriched lipoproteins (VLDL and LDL) is evident in rabbit heart

FTIR spectroscopy is based upon the interaction between the IR radiation and the covalent bonds of molecules. IR spectroscopy exploits the fact that molecules have specific frequencies at which they vibrate corresponding to discrete energy levels (vibrational modes). C-H stretching vibrations arise essentially from lipids and lead to absorption bands in the 3050–2800 cm^{-1}. In this infrared zone [3050–2800 cm^{-1}] of the FTIR spectra, human and rabbit lipoproteins showed the specific absorption of asymmetric and symmetric (CH3) and (CH2) stretching, mainly associated with the vibrational answer of the different classes of lipids, as well as the (C═H) stretching at 3010 cm^{-1} that corresponds to unsaturated lipids (Fig. S4a). The band associated with unsaturated lipids as well as the specific bands of CE in the [2900–2880 cm^{-1}] zone were better detected on the second derivative spectra (Fig. S4b) that enhances resolution for both lipoproteins and rabbit hearts.

In the [3050–2800 cm^{-1}] zone, the spectral signatures of lipids from LDL and VLDL were identified in the FTIR profile of hearts from both chow and HFD rabbit groups (Fig. 4a, Fig. S4a,b). These absorption bands can be detected at the same position both in lipoproteins and heart tissues. This fact indicates that these lipoproteins are one of the main sources of neutral lipids to the heart.

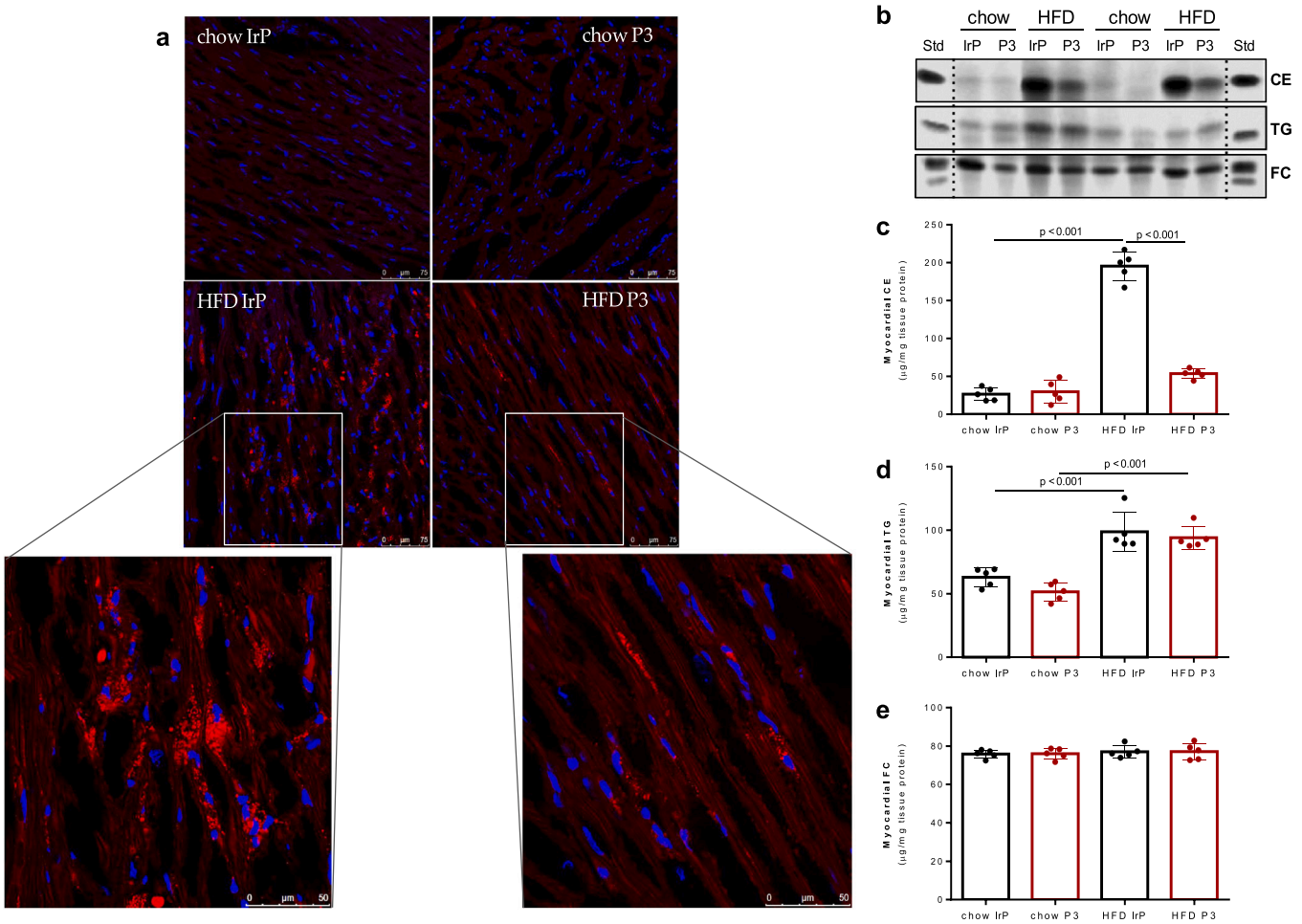

Fig. 2. Anti-P3 Abs specifically block the selective uptake of CE from lipoproteins in the heart. (a) Confocal microscopy images showing BODIPY-stained lipid droplets (*red dots*) in the hearts from the distinct rabbit groups. Cell nuclei are stained with DAPI (blue). (b) Representative TLC of heart lipid extracts and bands corresponding to the cardiac content of cholesteryl esters (CE), triglyceride (TG), and free cholesterol (FC). The CE/TG/FC bands of standards (Std) are shown in duplicate. Bar graph represents the mean ± SD of CE (c), TG (d), or FC (e), expressed as µg/mg tissue protein. Statistical significance was determined by 2-way ANOVA with Tukey's post-hoc test. $n = 5$/group. (For interpretation of the references to colour in this figure, the reader is referred to the web version of this article.)

3.5. Lipoprotein-derived CE accumulation in heart and HL-1 cardiomyocytes is reduced by anti-P3 Abs

Confocal microscopy analysis of BODIPY-stained transversal cross sections from the heart showed lower levels of lipid droplets in the HFD P3 group as compared to HFD IrP group (Fig. 2a). To further explore the impact of P3 immunization of cardiac lipid content, we performed thin-layer chromatography (TLC) of cardiac lipid extracts. TLC showed that HFD strongly increased intramyocardial CE and TG content as compared to chow diet (Fig. 2b–d). P3 immunization showed efficacy in reducing exclusively intramyocardial CE (Fig. 2b,c) but not TG content (Fig. 2b, d). Cardiac FC was similar for all four groups (Fig. 2b, e). Additionally, in *ex vivo* experiments, we explored the effect of increased percentages of serum (0.25–1 %; 1.5 h) from all four groups in the intracellular lipid content of the HL-1 cardiomyocytes. At 1.5 h, HFD serum induced intracellular CE/FC ratio in a dose-dependent manner but no changes in the TG/FC ratio. The anti-P3 Abs present in HFD P3 rabbit serum efficiently blocked the intracellular CE/FC ratio induced by the hypercholesterolemic serum in HL-1 cells at each tested dose (Fig. S5a,b).

3.6. P3 immunization changes the ultrastructure and bioenergetics of lipid droplets in the rabbit heart

Transmission electron microscopy (TEM) of ultrathin sections from heart of HFD-fed rabbits revealed the presence of neutral lipids forming lipid-filled vacuoles in cardiomyocytes of hearts from HFD groups (Fig. 3a,b and S6c,d). These lipid droplets were located between the sarcomere fibers and surrounded by a membrane that seems to be in close contact with mitochondria, as well as by the sarcoplasmic reticulum membrane. An important finding from electron microscopy studies was that lipid droplets in the heart of P3-immunized rabbits (Fig. 3b and S6d) were scarcer, more electrodense and bigger than those found in the heart of IrP injected rabbits (Fig. 3a and S6c). Another important finding was that the inter-sarcomere cytoplasm contained abundant glycogen in proximity with lipid droplets in the heart of HFD IrP (Fig. 3a and S6c) but not in that from HFD P3 rabbits (Fig. 3b and S6d). Similar or even higher abundance of glycogen drops were observed in the surroundings of lipid droplets formed in HL-1 cells exposed to rabbit HFD IrP serum (Fig. S7a, S7b). Lipid droplets were not detected in HL-1 cells exposed to rabbit serum from the other groups.

3.7. Anti-P3 Abs increase membrane InsR levels and restore InsR/LRP1 interaction and insulin signaling impaired by HFD in cardiomyocytes

We then evaluated InsR and LRP1 protein levels in the cardiac membranes and total extracts from the heart of the four different groups. Plasma membrane was disrupted by digitonin fractionation [36], and ATP1A1 (ATPaseNa/K) used as a specific marker for plasma membrane. As shown in Fig. 4a,b, membrane to total InsR ratio was significantly lower in the heart from HFD rabbits compared to than from chow rabbits, however, in the presence of anti-P3 Abs, membrane to total InsR ratio was restored and even exceeded those observed in chow rabbits. As shown in Fig. 4c,d, membrane to total LRP1 ratio was much higher in HFD than in control chow groups without differences between IrP and P3 groups. In addition, immunoprecipitation assays showed that InsR/LRP1 interaction complexes were reduced in the heart of HFD compared to chow groups; and that anti-P3 Abs not only restored but even surpassed the basal levels of InsR/LRP1 complexes observed in the heart of chow animals (Fig. 4e,f). Along the same line, *ex-vivo* experiments showed that treatment of HL-1 cardiomyocytes with HFD IrP serum reduced InsR/LRP1 complex levels in the absence or presence of insulin while HFD P3 serum restored and even increased the levels of InsR/LRP1 complex in these cells (Fig. S8a,b).

Confocal microscopy experiments showed that serum from HFD IrP animals, but not that from HFD P3 animals, reduced InsR and LRP1 colocalization in HL-1 cardiomyocytes (Fig. 5a,b). In addition, HFD IrP serum significantly reduced insulin-induced Akt and AS160 phosphorylation, while HFD P3 serum restored insulin-induced p-Akt and p-AS160 levels to those found in HL-1 cells exposed to chow serum (Fig. 5c-e). Taken together, these results indicate that anti-P3 Abs reduced the deleterious effect of HFD on the InsR/LRP1 association, InsR membrane translocation, and InsR signaling in cardiomyocytes.

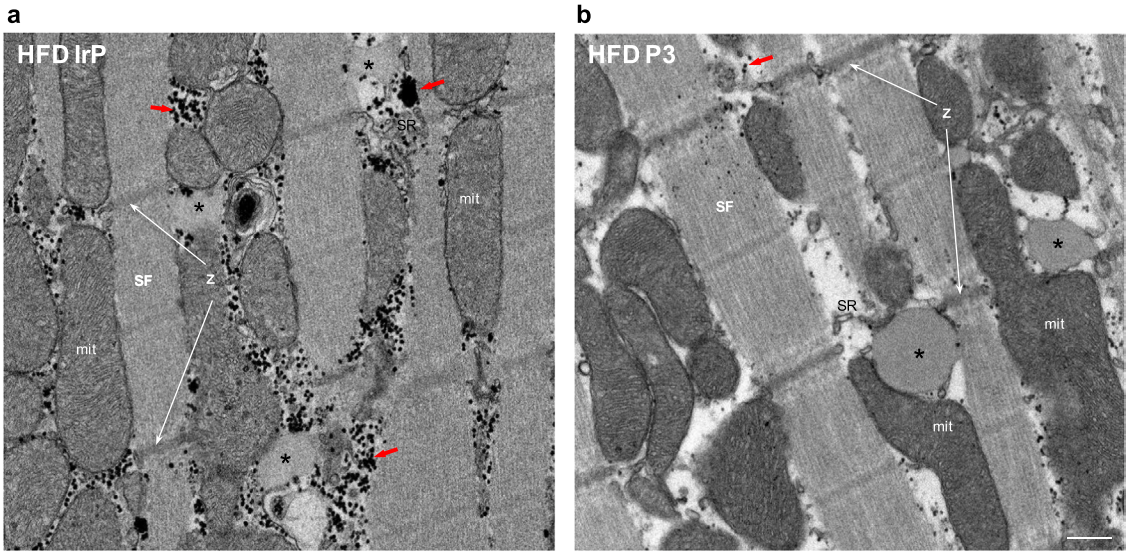

Fig. 3. Anti-P3 Abs alters lipid droplet size and electrodensity as well as the glycogen content induced by HDF. Representative electron microscopy of cardiomyocyte ultrastructure from the heart of HFD-fed rabbits showing differences between the size and electrodensity of lipid droplets (LD) (asterisks) in HFD IrP (a) and HFD P3 (b) rabbit groups. LD are located in the intersarcomeric cytoplasm between the sarcomeric fibers (SF) and in close connection with mitochondria (mit) and sarcoplasmic reticulum (SR). A high number of glycogen (electrodense granules, red arrows) surrounding the LD (asterisks) can also be observed in the heart of HFD IrP group. Representative Z-disc (Z) are indicated. Scale bar: 400 nm. (For interpretation of the references to colour in this figure, the reader is referred to the web version of this article.)

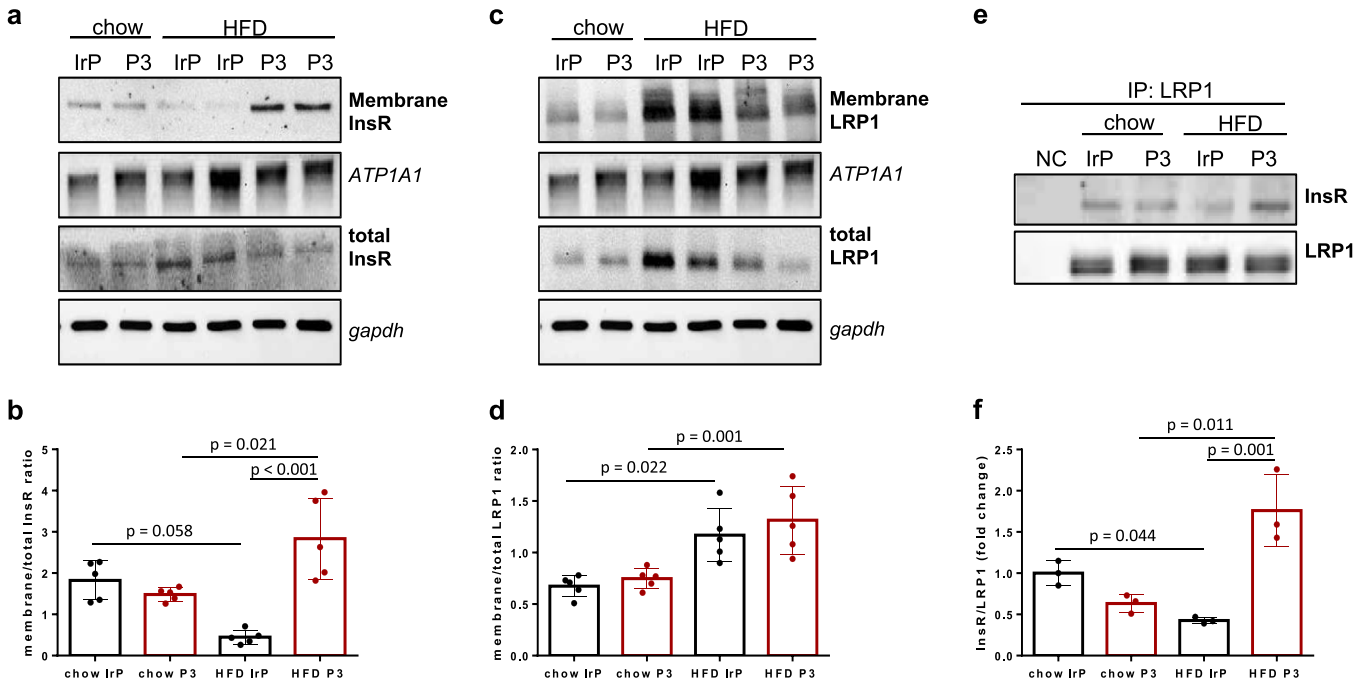

Fig. 4. Anti-P3 Abs prevent the deleterious effects of HFD on cardiac LRP1 and InsR membrane localization and interaction. Representative Western blot analysis of InsR (a) and LRP1 (c) in cardiac membranes and total cardiac lysates. Bar graph showing the InsR (b) and LRP1 (d) ratio between membrane and total levels normalized by ATP1A1 (membranes) or GAPDH (total extracts). $n = 5$/group. (e) Immunoprecipitation assay for LRP1. Myocardial lysates were immunoprecipitated with anti-LRP1 antibodies and analyzed by Western blot assays for InsR and total LRP1. NC, non-immune control without anti-LRP1 Ab. (f) Bar graph showing the densitometry quantification of Western blot bands. Values are expressed as mean ± SD of the relative intensity of LRP1 and InsR bands with respect to the endogenous control and are shown as a fold-change against the mean value of control IrP-immunized group. $n = 3$/group. Statistical significance was determined by 2-way ANOVA with Tukey's post-hoc test.

3.8. Anti-P3 Abs restore GLUT4 membrane levels in HFD hearts and the insulin response in HL-1 cardiomyocytes exposed to HFD serum

Western blot analysis (using ATP1A1 as a specific marker for plasma membrane) and confocal microscopy revealed that membrane to total GLUT4 ratio was much lower in the heart of HFD rabbits than in that of control chow rabbits, however, in the presence of anti-P3 Abs, GLUT4 membrane levels were restored to those observed in control chow rabbits (Fig. 6a-c). In addition, we evaluated whether anti-P3 Abs could restore GLUT4 trafficking to plasma membrane and glucose uptake in HL-1 cardiomyocytes exposed to HFD serum. Biotin-labeling cell surface protein assays showed that insulin failed to induce GLUT4 translocation to the plasma membrane in HL-1 cells exposed to HFD IrP but not in cells exposed to HFD P3 and chow serums (Fig. 6a,b). In line, insulin failed to induce 2-deoxyglucose (2-NBDG) uptake in HL-1 cells exposed to HFD IrP serum but not in cells exposed to HFD P3 and chow serums (Fig. 6c). These results suggest that anti-P3 Abs counteract the deleterious effect of HFD on GLUT4 trafficking to plasma membrane and glucose uptake in cardiomyocytes Fig. 7.

4. Discussion

Here we show that CE accumulation within the heart in response to HFD is driven by LRP1. Immunization of the rabbit model against the P3 sequence of LRP1 is able to reverse myocardial CE accumulation independently of changes in the circulating lipid profile. Here, we also show that intramyocardial CE accumulation is linked to a deficiency of InsR and GLUT4 in cardiac membranes as well as to impaired LRP1/InsR interaction, both of which were recovered in hypercholesterolemic rabbits by inhibition of myocardial CE accumulation. In line, *ex vivo* experiments showed that rabbit hypercholesterolemic serum strongly induces intracellular CE accumulation in HL-1 cardiomyocytes, decreasing InsR signaling, insulin-induced GLUT4 translocation to plasma membrane and insulin-induced glucose uptake in these cells. All these outputs were significantly reduced in HL-1 cells exposed to hypercholesterolemic serums containing anti-P3 Abs. These novel findings show that cardiomyocyte intracellular CE accumulation plays a crucial role in impaired cardiac insulin response induced by diet, and that these alterations are efficiently reduced by exposure to antibodies against the P3 sequence of LRP1 CR9 domain.

Intramyocardial CE accumulation in the heart is promoted by ischemia [35,37,39], hypercholesterolemia [40], and obesity [38]. However, the clinical impact of intramyocardial CE accumulation (independently of TG accumulation) has not yet been investigated, even though experimental studies have consistently shown that the causes and consequences of intracellular CE and TG accumulation involve differential mechanisms and pathological consequences. TG accumulation is mainly caused by an imbalance between the rates of fatty acid (FA) entry and FA oxidation, and it usually occurs in parallel to accumulation of detrimental lipid intermediates, such as long-chain acyl--CoA, ceramides, and diacylglycerol, all of which impair insulin signaling and glucose use in the heart [41]. We and others have proposed that intramyocardial CE accumulation is caused by the uptake of CE-enriched lipoproteins through lipoprotein receptors [22,35,39]. Here, molecular studies revealed that intramyocardial CE accumulation is mainly caused by LRP1-mediated uptake of CE-enriched lipoproteins, since it is blocked in rabbit heart by anti-P3 Abs, similar to our previous results in neonatal rat ventricular myocytes and cardiac-derived HL-1 cells by RNA silencing approaches [22,35]. CE-enriched VLDLs and LDLs are large lipoproteins in rabbits that display lower affinity for the LDL receptor [42,43] but increased affinity for the LRP1 receptor [29].

Our electron microscopy studies revealed that the lipid droplets in cardiomyocytes of P3- injected rabbits, although lower in number, are bigger and more electrodense than those found in the heart of IrP-injected rabbits. These imaging results combined with molecular and biophysical studies suggest that lipid droplets in the heart of P3-

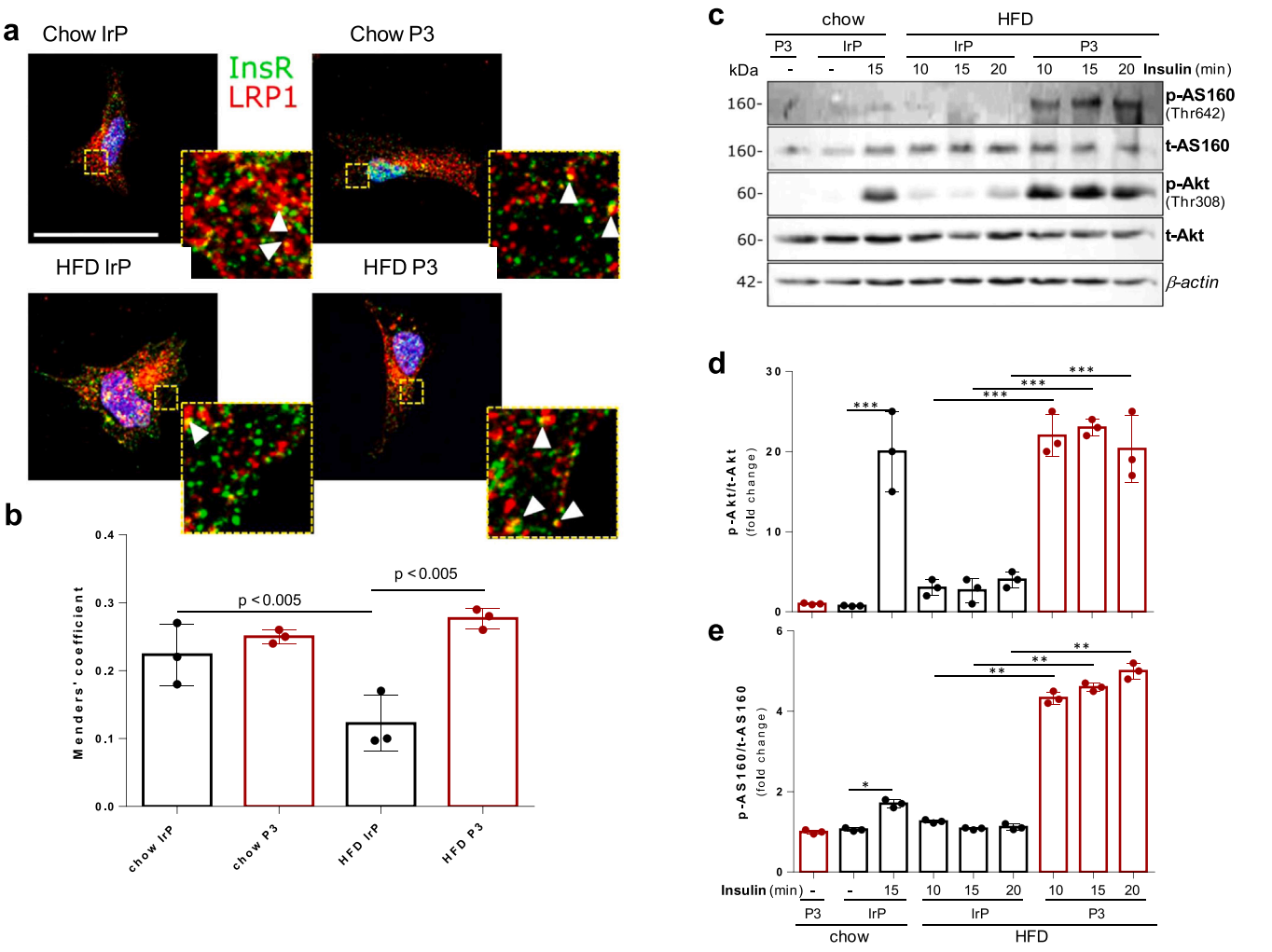

Fig. 5. Anti-P3 Abs block the down-regulatory effects of intracellular CE on InsR signaling in HL-1 cells. (a) Confocal microscopy of HL-1 cells exposed to rabbit serum (0.25 %, 1.5 h) from the different groups, showing the co-localization between LRP1 (red) and InsR (green). The inset represents the 4× magnification of the framed regions in the dotted lines. The white arrowheads indicate co-localization vesicles. Images are representative of three independent experiments ($n = 3$). Scale bar, 10 μm. (b) Bar graph showing the mean ± SD of Manders' coefficient of the co-localization between InsR and LRP1, obtained from the quantification performed in 30 cells per condition. (c) Western blot assays of phosphorylated Akt (p-Akt) and AS160 (p-AS160), and total Akt (t-Akt) and AS160 (t-AS160) in HL-1 cells exposed to serum (0.25 %, 1.5 h) from the different groups of rabbits and then stimulated with insulin (100 nM, 10–20 min). β-actin was used as a protein loading control. Bar graphs showing the densitometry quantification of p-Akt (d) and p-AS160 (e) normalized to t-Akt and t-AS160 bands respectively, and represented as a fold-change as compared to the mean of control IrP group. *** $p < 0.0001$ *versus* indicated conditions. ** $p < 0.001$ *versus* indicated conditions. Results are shown as mean ± SD of three independent experiments ($n = 3$). Statistical significance was determined by one-way ANOVA followed by a Dunnett's multiple comparison. (For interpretation of the references to colour in this figure, the reader is referred to the web version of this article.)

immunized rabbits contain almost exclusively TG, while those in the heart of IrP rabbits are mixed (cholesteryl esters and triglycerides). In line with our findings, lipid droplets containing exclusively CE have been observed to have a reduced size [44,45]. In addition, from the biophysical point of view, the liquid crystalline nature of CE mechanistically determines the intracellular phase behaviors of lipid droplets, and thus the structure and organization of a TG/CE lipid droplet, the lipid droplet nucleation, and the TG packaging [46,47]. These studies suggest that presence of CE limits lipid droplet growth, which would explain the smaller size of CE/TG lipid droplets present in the heart of the HFD IrP rabbits as compared to the TG-enriched lipid droplets present in the heart of HFD P3 rabbits. In addition, TLC results showed that P3- immunization had a strong efficacy in exclusively reducing intramyocardial CE content. Together, these results demonstrate that P3-immunization shows specificity for targeting CE accumulation in the heart.

Another key observation in this study is that mixed CE/TG lipid droplets formed in the heart of HFD rabbits and in HL-1 cells exposed to rabbit HFD IrP serum are surrounded by abundant glycogen drops, in contrast to TG-enriched lipid droplets in the heart of HFD P3 rabbits (which are not surrounded by glycogen). Our results suggest that P3-immunization counteracts the increased glycogen content induced by HFD in the heart of rabbits. Of note, previous studies have reported an increased glycogen content in the liver of fasted mice [48].

Our subfractionation studies combined with Western blot analysis showed that the membrane/total InsR ratio was lower in hearts from HFD rabbits than in those from normal chow rabbits. Coherently, LRP1 immunoprecipitation assays in rabbit heart tissue showed that HFD not only reduced cardiac membrane InsR levels but also disrupted InsR interaction with LRP1, suggesting that InsR/LRP1 interactions mainly occurs at the cardiac membrane. These results in the *in vivo* model are in line with previous studies from our group showing a reduction in the InsR/LRP1 association in aggregated LDL-loaded HL-1 cells [6]. It remains to be explored whether this interaction is direct or mediated by other intermediate proteins. A key result from the present study is that anti-P3 Abs, which blocked LRP1 interactions with CE-enriched

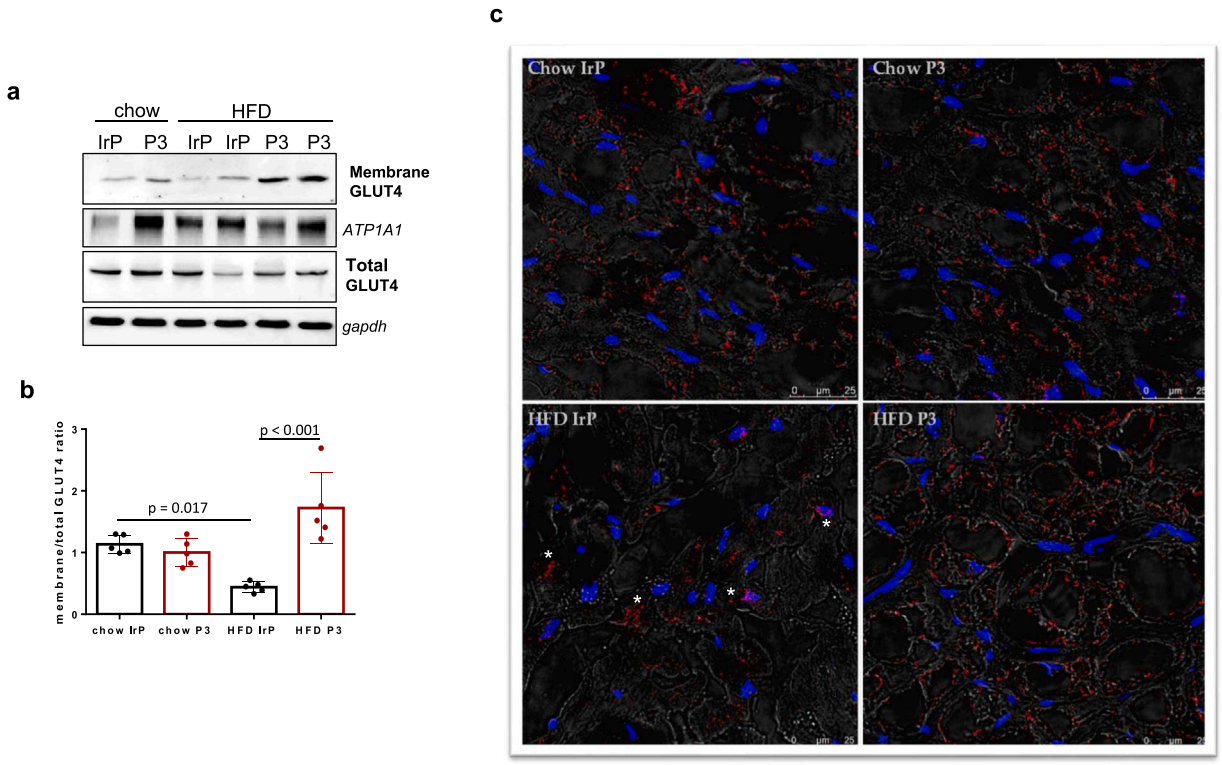

Fig. 6. Anti-P3 Abs block the deleterious effects of HFD on cardiac GLUT4 membrane localization. (a) Representative Western blot analysis of GLUT4 levels in cardiac membrane and total rabbit heart extracts. ATP1A1 and GADPH were used as protein loading controls for plasma membrane and total cardiac protein extracts, respectively. (b) Bar graphs showing the GLUT4 ratio between membrane and total levels normalized by ATP1A1 (membranes) or GADPH (total extracts), respectively. $n = 5$/group. (c) Confocal microscopy of slides from the heart of the four groups. Images show the localization of GLUT4 (in red) in cardiomyocytes. An overlay of confocal and transmission images helps to visualize GLUT4 localization in the boundary of cardiomyocytes in the hearts from the chow IrP, chow P3, and HFD P3 groups but not from HFD IrP rabbit group. Asteriks indicate GLUT4 in the cytoplasm of cardiomyocytes. Nuclei are shown in blue. (For interpretation of the references to colour in this figure, the reader is referred to the web version of this article.)

lipoproteins and intramyocardial CE accumulation, facilitated the recovery of InsR levels and InsR/LRP1 complex in membranes in the heart of rabbits and HL-1 cells exposed to HFD serum. Unexpectedly, we have also found that HFD increased total InsR levels in rabbit heart, and that anti-P3 Abs also blocked this effect. Interestingly, the presence of excessive InsR levels in muscle tissues has been proposed to contribute to dyslipemia and steatosis [49] and to be a compensatory mechanism in a situation of the HFD-generated insulin resistance [50].

In our model, both total and membrane LRP1 were higher in HFD-fed groups as compared to standard chow control groups, and anti-P3 Abs reduced the LRP1 levels to near that found in the control group, as expected by the positive transcriptional upregulation of LRP1 by hypercholesterolemia [51]. In the presence of anti-P3 Abs, the cardiac membrane InsR levels and the InsR/LRP1 interactions were even higher than those found in the control group, suggesting that blocking LRP1 interactions with lipoproteins could be a highly efficient process for recovering a correct cardiac insulin response. Our *ex vivo* studies showed that reducing the levels of the InsR/LRP1 complexes by a HFD was directly responsible for alterations in InsR signaling, in agreement with previous studies showing the pivotal role of LRP1 in insulin-induced InsR phosphorylation [6,25,26]. Further studies are now required to determine how intramyocardial CE accumulation impairs InsR/LRP1 complex formation and, how anti-P3 Abs overcome this effect.

Insulin and glucose metabolism are tightly related, and glucose transport across the cell membrane is strongly influenced by membrane fluidity [52] and, modulated by cholesterol [53]. Our current results from *ex vivo* studies showed that hypercholesterolemic serum reduced insulin response in terms of glucose uptake, and that anti-P3 Abs restored this response. In rabbit hearts, we showed that GLUT4 trafficking to cardiac membrane was reduced in HFD IrP rabbits but recovered in HFD P3 rabbits. In line with our results, HFD-mediated membrane cholesterol loading seems to promote the loss of cortical actin filaments required for GLUT4 trafficking to the membrane (a hallmark of skeletal muscle insulin resistance) [54]. We showed that blocking intramyocardial CE accumulation with anti-P3 Abs was sufficient to restore insulin-induced InsR signaling, GLUT4 trafficking to plasma membrane, and glucose uptake by HL-1 cardiomyocytes. Thus, LRP1-mediated CE accumulation is an early and reversible mechanism linking HFD to altered insulin response. Indeed, the multiple roles for LRP1 in mediating lipoprotein uptake [51,55], InsR signaling [6,25], and GLUT4 trafficking [6,23] also underpin the link between the cardiomyocyte intracellular CE accumulation and cardiac insulin signaling abnormalities. It is tempting to suggest that LRP1 binding to CE-enriched lipoproteins prevents the LRP1 receptor from interacting with other receptors or transporters, such as InsR or GLUT4, respectively, and this precludes their movement to plasma membrane. Further studies are required to explore these crucial mechanistic aspects connecting LRP1-mediated intramyocardial CE accumulation and insulin resistance in peripheral tissues. As glucose uptake in the heart is largely controlled by insulin-sensitive mechanisms, insulin resistance is an obstacle for enhanced myocardial glucose utilization. In recent studies, the use of insulin-sensitizing agents, such as metformin or SGLT2 (sodium-glucose cotransporter 2) inhibitors, was shown to reduce the risk of cardiovascular death or hospitalizations for heart failure in patients with T2DM [56,57].

A crucial question that remains open in this study is why anti-P3 Abs protected against HFD-induced cardiac but not peripheral insulin resistance. Peripheral insulin resistance is considered to be caused by hepatic steatosis [58], and HFD feeding dramatically increased accumulation of both CE and TG in the liver of this rabbit model. Of note,

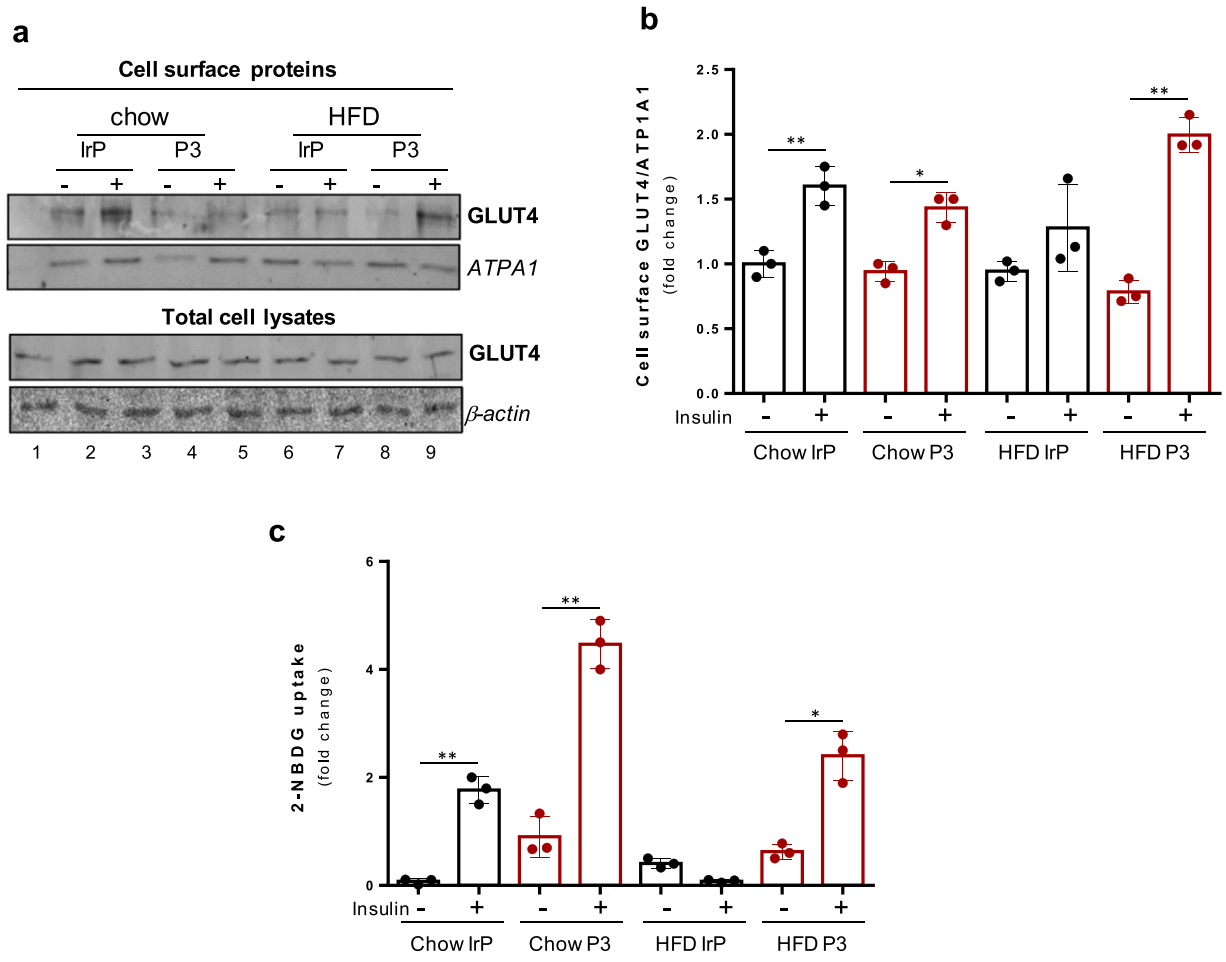

Fig. 7. Anti-P3 abs block the deleterious effects of hypercholesterolemic serum on GLUT4 traffic to the plasma membrane and glucose uptake by HL-1 cells. (a) Representative Western blot analysis from biotin-labeling protein assays of GLUT4 in the plasma membrane (upper panel) and in total cell extracts (lower panel) of HL-1 cells exposed to rabbit serum (0.25 %, 1.5 h) and stimulated with insulin (100 nM, 30 min). ATP1A1 and β-actin were used as protein loading controls for plasma membrane and total cell protein extracts, respectively. Line 1 represents control without biotin. (b) Bar graphs showing the quantification of Western blot bands for cell surface GLUT4 normalized to ATP1A1, and expressed as a fold-change as compared to the mean value of HL-1 exposed to serum from chow IrP group. Values are expressed as mean ± SD of three independent experiments ($n = 3$). (**c**) Bar graph showing the 2-NBDG uptake in HL-1 cells exposed to serum (0.25 %, 1.5 h) and then stimulated with insulin (100 nM, 30 min) in the presence of 2-NBDG (80 μM). The bar graph shows the mean ± SD of the fluorescence intensity of 2-NBDG per area of three independent experiments ($n = 3$), expressed as fold change as compared to the mean value of control IrP group. * $p < 0.05$; ** $p < 0.01$ insulin-stimulated *versus* basal. Statistical significance was determined by two-way ANOVA followed by a Student *t*-test.

hepatic TGs are the main regulators of VLDL secretion by the liver [59]. Controversially, insulin resistance has been reported to decrease membrane LRP1 levels in the liver, which could contribute to impaired hepatic clearance of triglyceride-rich lipoproteins. We now show that anti-P3 Abs had not protective effect against hepatic TG or CE accumulation induced by HFD. Importantly, anti-P3 Abs blocked the interaction of vascular LRP1 with ApoB100-enriched lipoproteins [29], the main lipoprotein ligand of LRP1 in the cardiovascular system. However, in liver, the main lipoprotein ligands of LRP1 are ApoE-enriched lipoproteins, such as chylomicrons [60]. It is known that ApoB100 and ApoE interact with the LRP1 receptor through domains localized in different clusters: CR9 in cluster II for ApoB100 [28] and CR17 in cluster IV for ApoE [61]. The inefficiency of anti-P3 Abs to block the interactions of LRP1 with ApoE-enriched lipoproteins could be the reason behind their lack of effect on HFD-induced systemic insulin resistance in rabbits.

In conclusion, our study now shows that i) diet-induced intramyocardial CE accumulation impaired cardiac insulin response, and that ii) anti-P3 Abs specifically and efficiently blocked intramyocardial CE accumulation, thereby normalizing the cardiac insulin response (summarized in Fig. 8). Further studies are required to determine the mechanisms underlying the link between reduced CE accumulation in the heart and restored insulin response. This aspect deserves to be investigated indepth given the potential role of myocardial CE accumulation on insulin resistance in a wide range of cardiac diseases. The innovative immunization-based approach that we took here, which differs from more traditional pharmacological or genetic techniques, showed both specificity and selectivity for targeting cardiovascular CE accumulation. These findings have important therapeutic implications in the management of CVD and shed new light on the complex role of LRP1 in regulating cardiac insulin response associated with hypercholesterolemia, obesity, and T2DM.

Research in context

Evidence before this study

Cardiovascular disease, the leading cause of death worldwide, is frequently associated with increased levels of atherogenic lipoproteins. Cholesteryl ester (CE)-enriched lipoproteins are an essential source of lipids to the heart; however, their dysregulated uptake and consequent lipid accumulation in the heart contributes to cardiac metabolic alterations and cardiac dysfunction. In particular, CE accumulation in the

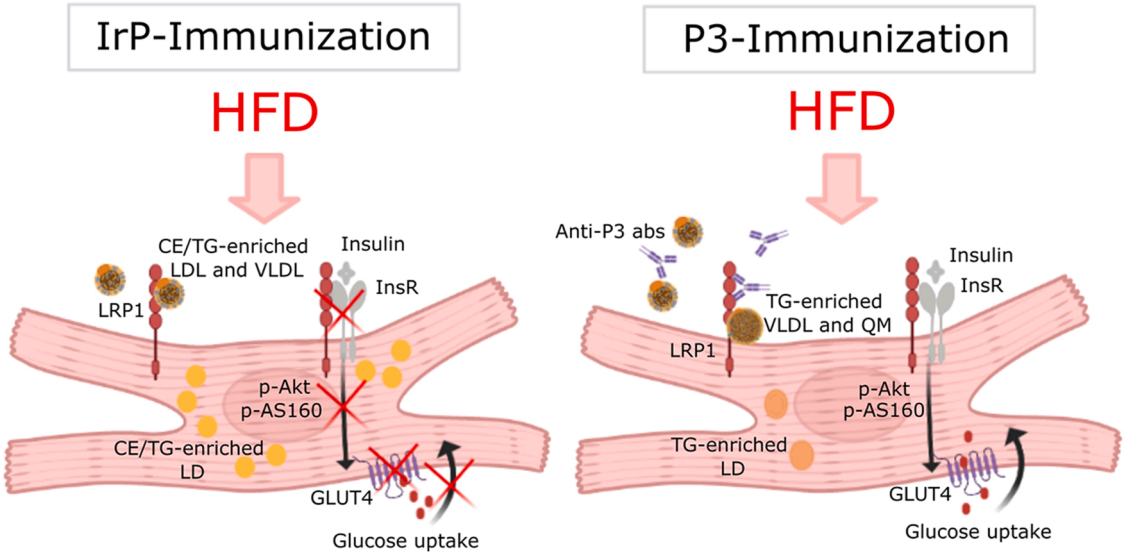

Fig. 8. Schematic summary of the main findings. A high-fat diet (HFD) causes a strong intramyocardial accumulation of cholesteryl ester (CE) associated with altered cardiac insulin response. By specifically blocking intramyocardial CE accumulation, P3 immunization restores insulin signaling and glucose uptake in cardiomyocytes.

heart causes calcium-handling alterations and cardiac remodeling in experimental models. Recently, a clinical study with more than 15,000 individuals has revealed the link between high levels of CE-enriched lipoproteins and left ventricle myocardial remodeling. Antibodies against the receptor LRP1 (the P3 sequence of CR9 domain of cluster II) specifically block intracellular CE accumulation in vascular cells by successful competition with aggregated LDL uptake. Moreover, P3 immunization of rabbits inhibits vascular CE accumulation and atherosclerosis.

Added value of this study

In this study, we used an innovative immunization-based approach to inhibit the CE uptake from lipoproteins into the heart. By complementary molecular, biophysical, and imaging approaches, we show that P3 immunization has specificity and selectivity for targeting intracellular CE accumulation within the heart of rabbits without modifying the circulating lipid profile or the myocardial triglyceride accumulation. In addition, we found that the selective inhibition of CE accumulation is enough to restore both the levels of InsR and GLUT4 levels in the cardiac membrane as well as the interaction between LRP1/InsR that is necessary for correct insulin signaling of hypercholesterolemic rabbits.

Implications of all the available evidence

This study provides new insight into lipid metabolism and its relationship to the insulin response in the heart and uncovers a novel and different approach to specifically modifying cholesterol metabolism and treat impaired cardiac insulin response. By providing a novel strategy of preventing the deleterious effect of hypercholesterolemia, it opens the possiblity for new therapeutical strategies of clinical management of impaired insulin response. Strikingly, reducing LRP1-mediated CE accumulation can restore insulin signaling in the myocardium. This is an important finding given the role of cardiac lipid accumulation and insulin response in a range of cardiac diseases and underscores the therapeutic potential/utility of antibody therapies.

Conflict of interest statement

The authors declare no conflict of interest.

Acknowledgements

The economic support to develop this project was received from Fundació MARATÓ TV3 with the grant 201521–10 (to V.Ll.-C), from the Instituto de Salud Carlos III (ISCIII) and co-financed with ERDFsFIS PI18/01584 (to V.Ll.-C), and from Fundación BBVA Ayudas a equipos de investigación 2019. This work was also funded by Secretaría de Ciencia y Tecnología de la Universidad Nacional de Córdoba (SECyT-UNC) grants PROYECTOS CONSOLIDAR 2018–2021 (to G.A.C); Fondo para la Investigación Científica y Tecnológica (FONCyT), Préstamo BID Proyecto de Investigación en Ciencia y Tecnología (PICT) grant 2015–0807 and grant 2017–4497 (to G.A.C). Support was received from Albert Renold Travel Fellowship Programme 2019 from the European Foundation of the study of Diabetes (EFSD) and the Wood-Whelan fellowship Programme 2019 from the International Union of Biochemistry and Molecular Biology (IUBMB) to cover the stay of V.A.D. in Institute of Biomedical Research of Barcelona (IIBB)-Spanish National Research Council (CSIC) and Biomedical Research Institute Sant Pau (IIB Sant Pau), Barcelona, Spain. V.A.D is a postdoctoral fellow of Consejo Nacional de Investigaciones Científicas y Técnicas (CONICET), Centro de Investigaciones en Bioquímica Clínica e Inmunología (CIBICI), Córdoba, Argentina. A.B.A. is a predoctoral fellow (FI19/00205) granted by the Programme _Contratos predoctorales de formación de investigación en salud_ from the Instituto de Salud Carlos III (ISCIII) and co-financed with ERDFs. Our group is part of CIBER Enfermedades Cardiovasculares (CIBERCV; CB16/11/00276 to J.M.G and VLl-C) and CIBER Diabetes y Enfermedades Metabólicas Asociadas (CIBERDEM; CB07/08/0016 to JCE-G), projects run by the Instituto de Salud Carlos III. Our group also participates in Redes de investigación (Enfermedades Metabóloicas y Cáncer RED2018–102799-T), a project run by MINECO. VLl-C group recognized by Generalitat de Catalunya (2017 SGR 946). We are thankful to Eva Prats and the staff from Centres Científics i Tecnològics de la Universitat de Barcelona (Campus Casanova) (CCiT/UB) for the processing of samples for electron microscopy. We also thank Veronica Raker for the scientitic and english editing of the manuscript.

Author contributions

V.A.D., and A.B.A contributed equally to this work. G.A.C. and V.Ll.-C. are both corresponding authors of this work. V.Ll.-C. and G.A.C. designed the research; V.A.D., A.B.A., E.G.,L.C; and M.T.L.C-H

performed most of the experimental research; A.I. contributed with the immunization procedure and ELISA design and setting to test anti-P3 Ab production in rabbits; JC.E.G contributed with biochemical determinations of lipoproteins; V.S. contributed with the biophysical analysis of lipoproteins and hearts; C.E. contributed with the electron microscopy experiments and images; V.A.D., A.B.A., J.M.G., G.A.C. and V.Ll.-C. analyzed the data; and V.A.D., G.A.C. and V.Ll.-C. wrote the paper.

Appendix A. Supporting information

Supplementary data associated with this article can be found in the online version at doi:10.1016/j.biopha.2022.113270.

References

[1] H. Bugger, E. Abel, Molecular mechanisms of diabetic cardiomyopathy, Diabetologia 57 (2014) 660–671, https://doi.org/10.1007/s00125-014-3171-6.

[2] C. Riehle, E. Abel, Insulin signaling and heart failure, Circ. Res. 118 (2016) 1151–1169, https://doi.org/10.1161/CIRCRESAHA.116.306206.

[3] M. Tadic, C. Cuspidi, D. Vasic, P.L.M. Kerkhof, Cardiovascular implications of diabetes, metabolic syndrome, thyroid disease, and cardio-oncology in women, Adv. Exp. Med. Biol. 1065 (2018) 471–488, https://doi.org/10.1007/978-3-319-77932-4_29.

[4] B. Bozkurt, D. Aguilar, A. Deswal, S.B. Dunbar, G.S. Francis, T. Horwich, et al., Contributory risk and management of comorbidities of hypertension, obesity, diabetes mellitus, hyperlipidemia, and metabolic syndrome in chronic heart failure: a scientific statement from the American Heart Association, Circulation 134 (2016) e535–e578, https://doi.org/10.1161/CIR.0000000000000450.

[5] W.B. Kannel, M. Hjortland, W.P. Castelli, Role of diabetes in congestive heart failure: the framingham study, Am. J. Cardiol. 34 (1974) 29–34, https://doi.org/10.1016/0002-9149(74)90089-7.

[6] V. Actis Dato, A. Benitez-Amaro, D. de Gonzalo-Calvo, M. Vazquez, G. Bonacci, V. Llorente-Cortés, et al., LRP1-mediated AggLDL endocytosis promotes cholesteryl ester accumulation and impairs insulin response in HL-1 Cells, Cells 9 (2020) 182, https://doi.org/10.3390/cells9010182.

[7] G. Jia, M.A. Hill, J.R. Sowers, Diabetic cardiomyopathy: an update of mechanisms contributing to this clinical entity, Circ. Res 122 (2018) 624–638, https://doi.org/10.1161/CIRCRESAHA.117.311586.

[8] Q. Hu, H. Zhang, N. Gutiérrez Cortés, D. Wu, P. Wang, J. Zhang, et al., Increased Drp1 Acetylation by Lipid Overload Induces Cardiomyocyte Death and Heart Dysfunction, Circ. Res 126 (2020) 456–470, https://doi.org/10.1161/CIRCRESAHA.119.315252.

[9] A. Ruiz-Ramírez, O. López-Acosta, M.A. Barrios-Maya, M. El-Hafidi, Cell death and heart failure in obesity: role of uncoupling proteins, Oxid. Med Cell Longev. 2016 (2016) 1–11, https://doi.org/10.1155/2016/9340654.

[10] G. Jia, V.G. DeMarco, J.R. Sowers, Insulin resistance and hyperinsulinaemia in diabetic cardiomyopathy, Nat. Rev. Endocrinol. 12 (2016) 144–153, https://doi.org/10.1038/nrendo.2015.216.

[11] N. Frangogiannis, Cardiac fibrosis, Cardiovasc Res 117 (2021) 1450–1488, https://doi.org/10.1093/cvr/cvaa324.

[12] M. Tate, D.J. Grieve, R.H. Ritchie, Are targeted therapies for diabetic cardiomyopathy on the horizon? Clin. Sci. (Lond.) 131 (2017) 897–915, https://doi.org/10.1042/CS20160491.

[13] N.G. Frangogiannis, The extracellular matrix in myocardial injury, repair, and remodeling, J. Clin. Invest 127 (2017) 1600–1612, https://doi.org/10.1172/JCI87491.

[14] M.R. Hayden, N. Chowdhury, G. Govindarajan, R. Poorna, P.R. Karuparthi, J. Habibi, et al., Myocardial myocyte remodeling and fibrosis in the cardiometabolic syndrome, J. Cardiometab Syndr. 1 (2007) 326–333, https://doi.org/10.1111/j.1559-4564.2006.05626.x.

[15] N. Aung, M.M. Sanghvi, S.K. Piechnik, S. Neubauer, P.B. Munroe, S.E. Petersen, The effect of blood lipids on the left ventricle, J. Am. Coll. Cardiol. 76 (2020) 2477–2488, https://doi.org/10.1016/j.jacc.2020.09.583.

[16] M. Ruuth, S.D. Nguyen, T. Vihervaara, M. Hilvo, T.D. Laajala, P.K. Kondadi, et al., Susceptibility of low-density lipoprotein particles to aggregate depends on particle lipidome, is modifiable, and associates with future cardiovascular deaths, Eur. Heart J. 39 (2018) 2562–2573, https://doi.org/10.1093/eurheartj/ehy319.

[17] C. Bancells, S. Villegas, F.J. Blanco, S. Benítez, I. Gállego, L. Beloki, et al., Aggregated electronegative low density lipoprotein in human plasma shows a high tendency toward phospholipolysis and particle fusion, J. Biol. Chem. 285 (2010) 32425–32435, https://doi.org/10.1074/jbc.M110.139691.

[18] E. Hurt-Camejo, G. Camejo, P. Sartipy, Phospholipase A2 and small, dense low-density lipoprotein, Curr. Opin. Lipido 11 (2000) 465–471, https://doi.org/10.1097/00041433-200010000-00004.

[19] G. Camejo, E. Hurt-Camejo, O. Wiklund, G. Bondjers, Association of apo B lipoproteins with arterial proteoglycans: pathological significance and molecular basis, Atherosclerosis 139 (1998) 205–222, https://doi.org/10.1016/S0021-9150(98)00107-5.

[20] V. Llorente-Cortés, M. Otero-Viñas, E. Hurt-Camejo, J. Martínez-González, L. Badimon, Human coronary smooth muscle cells internalize versican-modified LDL through LDL receptor–related protein and LDL receptors, Arterioscler. Thromb. Vasc. Biol. 22 (2002) 387–393, https://doi.org/10.1161/hq0302.105367.

[21] V. Llorente-Cortés, J. Martínez-González, L. Badimon, LDL receptor–related protein mediates uptake of aggregated LDL in human vascular smooth muscle cells, Arterioscler. Thromb. Vasc. Biol. 20 (2000) 1572–1579, https://doi.org/10.1161/01.ATV.20.6.1572.

[22] R. Cal, O. Juan-Babot, V. Brossa, S. Roura, C. Gálvez-Montón, M. Portoles, et al., Low density lipoprotein receptor-related protein 1 expression correlates with cholesteryl ester accumulation in the myocardium of ischemic cardiomyopathy patients, J. Transl. Med 10 (2012) 160, https://doi.org/10.1186/1479-5876-10-160.

[23] M.P. Jedrychowski, C.A. Gartner, S.P. Gygi, L. Zhou, J. Herz, K.V. Kandror, et al., Proteomic analysis of GLUT4 storage vesicles reveals LRP1 to Be an important vesicle component and target of insulin signaling, J. Biol. Chem. 285 (2010) 104–114, https://doi.org/10.1074/jbc.M109.040428.

[24] D. Leto, A.R. Saltiel, Regulation of glucose transport by insulin: traffic control of GLUT4, Nat. Rev. Mol. Cell Biol. 13 (2012) 383–396, https://doi.org/10.1038/nrm3351.

[25] C. Liu, J. Hu, C. Tsai, M. Yue, H.L. Melrose, T. Kanekiyo, et al., Neuronal LRP1 regulates glucose metabolism and insulin signaling in the brain, J. Neurosci. 35 (2015) 5851–5859, https://doi.org/10.1523/JNEUROSCI.5180-14.2015.

[26] Y. Ding, X. Xian, W. Holland, S. Tsai, J. Herz, Low-density lipoprotein receptor-related protein-1 protects against hepatic insulin resistance and hepatic steatosis, EBioMedicine 7 (2016) 135–145, https://doi.org/10.1016/j.ebiom.2016.04.002.

[27] V. Actis Dato, R. Grosso, M.C. Sánchez, C.F. Fader, G.A. Chiabrando, Insulin-induced exocytosis regulates the cell surface level of low-density lipoprotein-related protein-1 in Müller Glial cells, Biochem J. 475 (2018) 1669–1685, https://doi.org/10.1042/BCJ20170891.

[28] P. Costales, P. Fuentes-Prior, J. Castellano, E. Revuelta-Lopez, M.A. Corral-Rodríguez, L. Nasarre, et al., K domain CR9 of low density lipoprotein (LDL) receptor-related protein 1 (LRP1) is critical for aggregated LDL-induced foam cell formation from human vascular smooth muscle cells, J. Biol. Chem. 290 (2015) 14852–14865, https://doi.org/10.1074/jbc.M115.638361.

[29] O. Bornachea, A. Benitez-Amaro, A. Vea, L. Nasarre, D. de Gonzalo-Calvo, J. C. Escola-Gil, et al., Immunization with the Gly 1127 -Cys 1140 amino acid sequence of the LRP1 receptor reduces atherosclerosis in rabbits. Molecular, immunohistochemical and nuclear imaging studies, Theranostics 10 (2020) 3263–3280, https://doi.org/10.7150/thno.37305.

[30] S. Toldo, D. Austin, A.G. Mauro, E. Mezzaroma, B.W. Van Tassell, C. Marchetti, et al., Low-density lipoprotein receptor–related protein-1 Is a therapeutic target in acute myocardial infarction, JACC: Basic Transl. Sci. 2 (2017) 561–574, https://doi.org/10.1016/j.jacbts.2017.05.007.

[31] N. Potere, M.G. del Buono, G. Niccoli, F. Crea, S. Toldo, A. Abbate, Developing LRP1 agonists into a therapeutic strategy in acute myocardial infarction, Int J. Mol. Sci. 20 (2019) 544, https://doi.org/10.3390/ijms20030544.

[32] S. Avrameas, Coupling of enzymes to proteins with glutaraldehyde, Immunochemistry 6 (1969) 43–52, https://doi.org/10.1016/0019-2791(69)90177-3.

[33] J. Julve, J.C. Escolà-Gil, N. Rotllan, C. Fiévet, E. Vallez, C. de la Torre, et al., Human apolipoprotein A-II determines plasma triglycerides by regulating lipoprotein lipase activity and high-density lipoprotein proteome, Arterioscler. Thromb. Vasc. Biol. 30 (2010) 232–238, https://doi.org/10.1161/ATVBAHA.109.198226.

[34] J.C. Escolà-Gil, G. Llaverias, J. Julve, M. Jauhiainen, J. Méndez-González, F. Blanco-Vaca, The cholesterol content of western diets plays a major role in the paradoxical increase in high-density lipoprotein cholesterol and upregulates the macrophage reverse cholesterol transport pathway, Arterioscler. Thromb. Vasc. Biol. 31 (2011) 2493–2499, https://doi.org/10.1161/ATVBAHA.111.236075.

[35] R. Cal, J. Castellano, E. Revuelta-López, R. Aledo, M. Barriga, J. Farré, et al., Low-density lipoprotein receptor-related protein 1 mediates hypoxia-induced very low density lipoprotein-cholesteryl ester uptake and accumulation in cardiomyocytes, Cardiovasc Res 94 (2012) 469–479, https://doi.org/10.1093/cvr/cvs136.

[36] I. Schulz, [19] Permeabilizing cells: Some methods and applications for the study of intracellular processes, Methods Enzym. 192 (1990) 280–300, https://doi.org/10.1016/0076-6879(90)92077-Q.

[37] V. Samouillan, I.M. Martinez de Lejarza Samper, A. Benitez-Amaro, D. Vilades, J. Dandurand, J. Casas, et al., Biophysical and lipidomic biomarkers of cardiac remodeling post-myocardial infarction in humans, Biomolecules 10 (2020) 1471, https://doi.org/10.3390/biom10111471.

[38] V. Samouillan, E. Revuelta-López, J. Dandurand, L. Nasarre, L. Badimon, C. Lacabanne, et al., Cardiomyocyte intracellular cholesteryl ester accumulation promotes tropoelastin physical alteration and degradation, Int J. Biochem Cell Biol. 55 (2014) 209–219, https://doi.org/10.1016/j.biocel.2014.09.005.

[39] C. Drevinge, L.O. Karlsson, M. Ståhlman, T. Larsson, J. Perman Sundelin, L. Grip, et al., Cholesteryl esters accumulate in the heart in a porcine model of ischemia and reperfusion, PLoS One 8 (2013), e61942, https://doi.org/10.1371/journal.pone.0061942.

[40] Y. Huang, K.E. Walker, F. Hanley, J. Narula, S.R. Houser, T.N. Tulenko, Cardiac systolic and diastolic dysfunction after a cholesterol-rich diet, Circulation 109 (2004) 97–102, https://doi.org/10.1161/01.CIR.0000109213.10461.F6.

[41] A. Gastaldelli, M.A. Morales, P. Marraccini, R. Sicari, The role of cardiac fat in insulin resistance, Curr. Opin. Clin. Nutr. Metab. Care 15 (2012) 523–528, https://doi.org/10.1097/MCO.0b013e328358be7b.

[42] F. Nigon, P. Lesnik, M. Rouis, M.J. Chapman, Discrete subspecies of human low density lipoproteins are heterogeneous in their interaction with the cellular LDL

receptor, J. Lipid Res 32 (1991) 1741–1753, https://doi.org/10.1016/S0022-2275(20)41629-3.
[43] J.R. McNamara, D.M. Small, Z. Li, E.J. Schaefer, Differences in LDL subspecies involve alterations in lipid composition and conformational changes in apolipoprotein B, J. Lipid Res 37 (1996) 1924–1935, https://doi.org/10.1016/S0022-2275(20)37557-X.
[44] W. Shen, S. Azhar, F. Kraemer, Lipid droplets and steroidogenic cells, Exp. Cell Res. 340 (2016) 209–214, https://doi.org/10.1016/j.yexcr.2015.11.024.
[45] X. Zhou, Z. Mo, Y. Li, L. Huang, S. Yu, L. Ge, Y. Hu, S. Shi, L. Zhang, L. Wang, L. Gao, G. Yang, G. Chu, Oleic acid reduces steroidogenesis by changing the lipid type stored in lipid droplets of ovarian granulosa cells, J. Anim. Sci. Biotechnol. 13 (2022) 27, https://doi.org/10.1186/s40104-021-00660-5.
[46] V. Zoni, R. Khaddaj, P. Campomanes, A. Thiam, R. Schneiter, S. Vanni, Pre-existing bilayer stresses modulate triglyceride accumulation in the ER versus lipid droplets, eLife (2021) 10, https://doi.org/10.7554/eLife.62886.
[47] S.F. Shimobayashi, Y. Ohsaki, Universal phase behaviors of intracellular lipid droplets, PNAS 116 (2019) 25440–25445, https://doi.org/10.1073/pnas.1916248116.
[48] B. Lu, D. Bridges, Y. Yang, K. Fisher, A. Cheng, L. Chang, et al., Metabolic crosstalk: molecular links between glycogen and lipid metabolism in obesity, Diabetes 63 (2014) 2935–2948, https://doi.org/10.2337/db13-1531.
[49] R.K. Semple, A. Sleigh, P.R. Murgatroyd, C.A. Adams, L. Bluck, S. Jackson, et al., Postreceptor insulin resistance contributes to human dyslipidemia and hepatic steatosis, J. Clin. Invest 119 (2009) 315, https://doi.org/10.1172/JCI37432.
[50] G. Wang, Y. Yu, W. Cai, T.M. Batista, S. Suk, H.L. Noh, et al., Muscle-specific insulin receptor overexpression protects mice from diet-induced glucose intolerance but leads to postreceptor insulin resistance, Diabetes 69 (2020) 2294–2309, https://doi.org/10.2337/db20-0439.
[51] V. Llorente-Cortés, M. Otero-Viñas, S. Sánchez, C. Rodríguez, L. Badimon, Low-density lipoprotein upregulates low-density lipoprotein receptor-related protein expression in vascular smooth muscle cells, Circulation 106 (2002) 3104–3110, https://doi.org/10.1161/01.CIR.0000041434.28573.0B.
[52] N. Al-Makdissy, M. Younsi, S. Pierre, O. Ziegler, M. Donner, Sphingomyelin/cholesterol ratio: an important determinant of glucose transport mediated by GLUT-1 in 3T3-L1 preadipocytes, Cell Signal 15 (2003) 1019–1030, https://doi.org/10.1016/s0898-6568(03)00070-6.
[53] N. Saxena, N.C. Chandra, Cholesterol: a prelate in cell nucleus and its serendipity, Curr. Mol. Med. 20 (2021) 692–707, https://doi.org/10.2174/1566524020666200413112030.
[54] K.M. Habegger, B.A. Penque, W. Sealls, L. Tackett, L.N. Bell, E.K. Blue, et al., Fat-induced membrane cholesterol accrual provokes cortical filamentous actin destabilisation and glucose transport dysfunction in skeletal muscle, Diabetologia 55 (2012) 457–467, https://doi.org/10.1007/s00125-011-2334-y.
[55] V. Llorente-Cortés, M. Otero-Viñas, S. Camino-López, P. Costales, L. Badimon, Cholesteryl esters of aggregated LDL are internalized by selective uptake in human vascular smooth muscle cells, Arterioscler. Thromb. Vasc. Biol. 26 (2006) 117–123, https://doi.org/10.1161/01.ATV.0000193618.32611.8b.
[56] J.M.M. Evans, A.S.F. Doney, M.A. AlZadjali, S.A. Ogston, J.R. Petrie, A.D. Morris, et al., Effect of metformin on mortality in patients with heart failure and type 2 diabetes mellitus, Am. J. Cardiol. 106 (2010) 1006–1010, https://doi.org/10.1016/j.amjcard.2010.05.031.
[57] M. Packer, Reconceptualization of the molecular mechanism by which sodium-glucose cotransporter 2 inhibitors reduce the risk of heart failure events, Circulation 140 (2019) 443–445, https://doi.org/10.1161/CIRCULATIONAHA.119.040909.
[58] C. Postic, R. Dentin, J. Girard, Role of the liver in the control of carbohydrate and lipid homeostasis, Diabetes Metab. 30 (2004) 398–408, https://doi.org/10.1016/S1262-3636(07)70133-7.
[59] B.C. Moon, A. Hernandez-Ono, B. Stiles, H. Wu, H.N. Ginsberg, Apolipoprotein B secretion is regulated by hepatic triglyceride, and not insulin, in a model of increased hepatic insulin signaling, Arterioscler. Thromb. Vasc. Biol. 32 (2012) 236–246, https://doi.org/10.1161/ATVBAHA.111.241356.
[60] A. Rohlmann, M. Gotthardt, R.E. Hammer, J. Herz, Inducible inactivation of hepatic LRP gene by cre-mediated recombination confirms role of LRP in clearance of chylomicron remnants, J. Clin. Invest 101 (1998) 689–695, https://doi.org/10.1172/JCI1240.
[61] M. Guttman, J.H. Prieto, J.E. Croy, E.A. Komives, Decoding of lipoprotein−receptor interactions: properties of ligand binding modules governing interactions with apolipoprotein E, Biochemistry 49 (2010) 1207–1216, https://doi.org/10.1021/bi9017208.